AGU PUBLICATIONS

JGR

Journal of Geophysical Research: Atmospheres

RESEARCH ARTICLE
10.1002/2014JD022993

Key Points:
- Multi-scale assimilation reassessed O_3 source contributions in CA and NV
- Background/total O_3 varied in high-elevation remote areas and flat urban areas
- Background O_3 in five subregions on days of O_3 exceedances was computed

Correspondence to:
M. Huang,
mhuang10@gmu.edu

Citation:
Huang, M., K. W. Bowman, G. R. Carmichael, M. Lee, T. Chai, S. N. Spak, D. K. Henze, A. S. Darmenov, and A. M. da Silva (2015), Improved western U.S. background ozone estimates via constraining nonlocal and local source contributions using Aura TES and OMI observations, *J. Geophys. Res. Atmos.*, *120*, doi:10.1002/2014JD022993.

Received 17 DEC 2014
Accepted 21 MAR 2015
Accepted article online 25 MAR 2015

Improved western U.S. background ozone estimates via constraining nonlocal and local source contributions using Aura TES and OMI observations

Min Huang[1,2,3], Kevin W. Bowman[1], Gregory R. Carmichael[4], Meemong Lee[1], Tianfeng Chai[5], Scott N. Spak[4,6], Daven K. Henze[7], Anton S. Darmenov[8], and Arlindo M. da Silva[8]

[1]Jet Propulsion Laboratory, California Institute of Technology, Pasadena, California, USA, [2]Now at Spatial Information Science and Systems Center, George Mason University, Fairfax, Virginia, USA, [3]Now at NOAA Center for Weather and Climate Prediction, College Park, Maryland, USA, [4]Center for Global and Regional Environmental Research, University of Iowa, Iowa City, Iowa, USA, [5]NOAA Air Resources Laboratory, College Park, Maryland, USA, [6]Public Policy Center, University of Iowa, Iowa City, Iowa, USA, [7]Department of Mechanical Engineering, University of Colorado, Boulder, Colorado, USA, [8]Global Modeling and Assimilation Office, NASA Goddard Space Flight Center, Greenbelt, Maryland, USA

Abstract Western U.S. near-surface ozone (O_3) concentrations are sensitive to transported background O_3 from the eastern Pacific free troposphere, as well as U.S. anthropogenic and natural emissions. The current 75 ppbv U.S. O_3 primary standard may be lowered soon, hence accurately estimating O_3 source contributions, especially background O_3 in this region has growing policy-relevant significance. In this study, we improve the modeled total and background O_3, via repartitioning and redistributing the contributions from nonlocal and local anthropogenic/wildfires sources in a multi-scale satellite data assimilation system containing global Goddard Earth Observing System–Chemistry model (GEOS-Chem) and regional Sulfur Transport and dEposition Model (STEM). Focusing on NASA's ARCTAS (Arctic Research of the Composition of the Troposphere from Aircraft and Satellites) field campaign period in June–July 2008, we first demonstrate that the negative biases in GEOS-Chem free simulation in the eastern Pacific at 400–900 hPa are reduced via assimilating Aura-Tropospheric Emission Spectrometer (TES) O_3 profiles. Using the TES-constrained boundary conditions, we then assimilated into STEM the tropospheric nitrogen dioxide (NO_2) columns from Aura-Ozone Monitoring Instrument to indicate U.S. nitrogen oxides ($NO_x = NO_2 + NO$) emissions at $12 \times 12\ km^2$ grid scale. Improved model skills are indicated from cross validation against independent ARCTAS measurements. Leveraging Aura observations, we show anomalously high wildfire NO_x emissions in this summer in Northern California and the Central Valley while lower anthropogenic emissions in multiple urban areas than those representing the year of 2005. We found strong spatial variability of the daily maximum 8 h average background O_3 and its contribution to the modeled total O_3, with the mean value of ~48 ppbv (~77% of the total).

1. Introduction

Tropospheric ozone (O_3), either originating from the stratosphere [*Stohl et al.*, 2003] or photochemically produced in the troposphere [e.g., *Monks et al.*, 2009], affects atmospheric chemistry, human and ecosystem health, and the climate on local, regional, and global scales [*Smith et al.*, 2009; *Anenberg et al.*, 2010; *Avnery et al.*, 2011a, 2011b, 2013; *Ainsworth et al.*, 2012; *Bowman and Henze*, 2012; *Bowman et al.*, 2013; *Fishman et al.*, 2014; *Shindell et al.*, 2009, 2013; *Stevenson et al.*, 2013; *Cooper and Ziemke*, 2014]. Modifying O_3 distributions rapidly changes these impacts due to its short lifetimes ranging from hours in the boundary layer to longer than several weeks in the free troposphere [*Stevenson et al.*, 2006; *United Nations Environment Programme and World Meteorological Organization*, 2011; *Task Force on Hemispheric Transport of Air Pollution* (*TF HTAP*), 2010; *National Research Council* (*NRC*), 2009].

Ground-level O_3 is one of the six criteria air pollutants regulated by the U.S. Environmental Protection Agency (EPA) since the 1970s (http://www.epa.gov/airquality/ozonepollution/). The current U.S. O_3 primary and secondary national ambient air quality standards (NAAQS), which aim at protecting public health and sensitive ecosystems, respectively, are both set at 75 ppbv. Based on these standards, there still exist large O_3 nonattainment areas in California [*U.S. Environmental Protection Agency* (*EPA*), 2014; *The Green Book Nonattainment Areas for Criteria Pollutants*, 2014]. Ozone exceedances have also been observed in its neighboring state Nevada [*Jaffe et al.*, 2008, 2013; *Jaffe*, 2011; *Langford et al.*, 2014], a less

studied area with sparse surface monitoring sites. U.S. EPA is proposing to tighten the primary O_3 standard to within a range of 65 to 70 ppbv to better protect Americans' health and the environment while taking comment on a level as low as the European standard of 60 ppbv. The final O_3 standard will be issued in October 2015 (http://yosemite.epa.gov/opa/admpress.nsf/bd4379a92ceceeac8525735900400c27/6ce92be958c8149285257d9c0049562e!OpenDocument, accessed in November 2014). Expanded regions in California and Nevada are projected to violate the more stringent standard, and higher costs for reducing the O_3 levels are expected in response to these potential new thresholds [*McCarthy*, 2010].

Near-surface O_3 variability in California and Nevada is affected by pollutants transported from the free troposphere over the eastern Pacific, as well as the U.S.-emitted O_3 precursors from anthropogenic and natural sources [*Parrish et al*., 2010; *Huang et al*., 2010, 2013; *Lin et al*., 2012a, 2012b; *Pfister et al*., 2008; *Langford et al*., 2011; *Yates et al*., 2013, 2014; *NRC*, 2009]. Over the past few decades, observations indicate increasing O_3 trends in the free troposphere in the eastern Pacific and high-altitude remote sites in the western U.S. in spring and summer [e.g., *Cooper et al*., 2010, 2012, 2014; *Parrish et al*., 2009, 2012; *Gratz et al*., 2014]. This trend can be in part due to the increasing contributions from nonlocal sources such as transported Asian pollution, and it may be correlated to the O_3 variability in downwind inland regions [*Huang et al*., 2010; *Parrish et al*., 2010; *Cooper et al*., 2011; *Ambrose et al*., 2011; *Wigder et al*., 2013; *Yates et al*., 2014]. In contrast, decreasing trends in O_3 and its precursor species are found over the populated areas at low altitudes such as California's South Coast and part of the Central Valley [e.g., *Pollack et al*., 2013; *Parrish et al*., 2011; *Cooper et al*., 2014; *Pusede and Cohen*, 2012]. This reflects their stronger sensitivity to the decreasing local anthropogenic emissions as a result of effective local emission controls and the recent economic recession [e.g., *Russell et al*., 2010, 2012; *Warneke et al*., 2012; *McDonald et al*., 2012, 2013]. In addition, changes in land use and climate modify meteorological conditions such as temperature and water vapor, biogenic emissions [e.g., *Steiner et al*., 2006; *Camalier et al*., 2007], as well as the frequencies and emissions of wildfires [*Pechony and Shindell*, 2010; *van der Werf et al*., 2010], all of which can affect O_3 production. The U.S. "background O_3" (a model construct) and "baseline O_3" (a measured quantity) are often used interchangeably to inform the policy makers of the O_3 levels unaffected by recently emitted or produced anthropogenic emissions in the U.S. and to suggest how much O_3 from anthropogenic emission sources would be allowed for attaining the O_3 standards. The different trends and variability of the various O_3 contributors indicate that background and baseline O_3 tend to contribute to a greater proportion of ambient O_3 in recent years and future, and these contributions vary spatially [*McDonald-Buller et al*., 2011; *TF HTAP*, 2010; *NRC*, 2009]. Therefore, better evaluating the potential NAAQS can benefit from timely updating the estimates of O_3 pollution levels and its source contribution in various geographic regions (e.g., on state or county level) with improved accuracy.

Chemical transport models have been used to reproduce and attribute observed O_3 levels in the western U.S. [e.g., *TF HTAP*, 2010; *Zhang et al*., 2008; *Lin et al*., 2012a, 2012b; *Pfister et al*., 2008; *Wild and Prather*, 2006]. However, large intermodel diversity and wide ranges of model-observation discrepancies are often found, indicating challenges with pure model simulations [e.g., *Emery et al*., 2012; *Zhang et al*., 2011; *Fiore et al*., 2009, 2014; *Parrish et al*., 2014; *Lapina et al*., 2014]. One of the major sources of uncertainties comes from the emission inputs used in model simulations: The decreasing trends of U.S. and increasing non-U.S. anthropogenic emissions of O_3 precursors may not be well represented in the outdated bottom-up emission inventories being used, and estimates of emissions from some natural (e.g., wildfires, biogenic, and lightning) sources can be highly uncertain as they can be episodically strong and/or meteorological dependent. In addition, there are uncertainties in the treatment of transport, chemistry, and deposition, varying among the different used models.

Reducing the uncertainties of the modeled total and background O_3, as well as their source contributions, can benefit from integrating the observations over three dimensions into the modeling analysis via careful model validation and chemical data assimilation [e.g., *Bouttier and Courtier*, 1999; *Chai et al*., 2006, 2007; *Carmichael et al*., 2008; *Sandu and Chai*, 2011; *Parrington et al*., 2008, 2009; *Huang et al*., 2013, 2014]. Among the various types of available observations, satellite retrievals routinely provide broad geographic coverage for the distributions of O_3 and its key precursor species. In this study, we integrate observations from the NASA Aura satellite into a multi-scale chemical data assimilation system (Figure 1 and section 2)

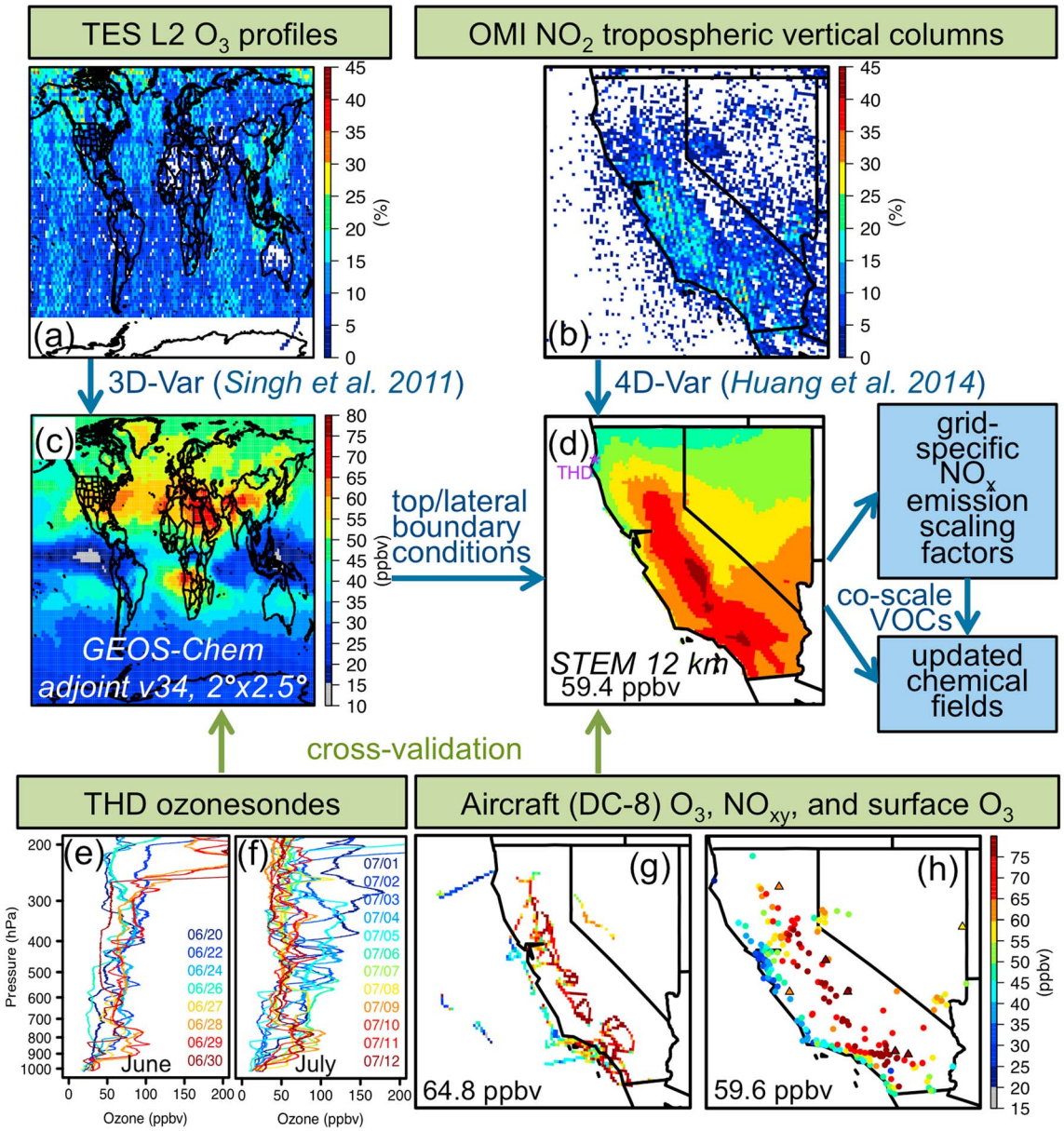

Figure 1. Methodology chart including the used observations, models, and assimilation methods: (a) TES sampling density (i.e., number of days that each grid had sample(s)/30 days) in GEOS-Chem grid and (b) OMI sampling density in STEM grid, period-mean modeled O_3 a posteriori at (c) GEOS-Chem level 16 (~750 hPa) and (d) STEM near-surface daytime (08:00–19:00 local standard time; <2 km agl); (e and f) ozonesondes at Trinidad Head (THD, location indicated in Figure 1d) in (Figure 1e) June and (Figure 1f) July 2008; and (g) the grid-averaged near-surface O_3 along six DC-8 daytime flight paths during the studied period. The flight paths on individual days are in Figure 2a. (h) Observed period-mean daily-maximum 8 h average O_3 at surface AQS (circle) and CASTNET (triangle) sites. Figures 1d, 1g, and 1h share the same color scale, and the domain-mean values are shown at the bottom left corner in each panel.

and aim to improve regional-modeled total and background O_3 distributions in California and Nevada, by sequentially constraining the contributions from nonlocal pollution (which approximates those transported through the regional model boundary) and local O_3 precursors' emissions from various sources (e.g., anthropogenic sources and wildfires). We focus on the "California" and "summer" phases of the NASA Arctic Research of the Composition of the Troposphere from Aircraft and Satellites (ARCTAS) field experiment from mid-June to mid-July 2008 [*Jacob et al.*, 2010]. Previous studies using the rich measurements collected during this campaign found that nonlocal pollutants were mixed with local pollution from various emission sources (e.g., urban anthropogenic and wildfires), causing expanded area

Table 1. Modeling/Assimilation Cases in This Study (Details Are in Sections 2.1 and 2.3)[a]

Case Name	Model	TES O_3 Constraints	OMI NO_2 Constraints	Base or Background
GC_F_BASE	GEOS-Chem			Base
GC_T_BASE	GEOS-Chem	✓		Base
GC_ScaleT_BASE (not used)	GEOS-Chem	✓		Base
STEM_F_BASE	STEM			Base
STEM_T_BASE	STEM	✓		Base
STEM_TO_BASE	STEM	✓	✓	Base
STEM_F_BKG	STEM			Background
STEM_T_BKG	STEM	✓		Background
STEM_TO_BKG	STEM	✓	✓	Background

[a]Each case name is composed of three parts separating by two underscore symbols, and they refer to the used model (GEOS-Chem (GC) or STEM), any observation constraints (F: free run, T: with TES constraints, and TO: with TES and OMI constraints), and whether it is a base (including all emission sectors) or a background (no anthropogenic) simulation.

of O_3 exceedances in California [*Singh et al*., 2010, 2012; *Huang et al*., 2010, 2013; *Pfister et al*., 2011]. These available nonassimilated in situ (balloon-borne, airborne, and surface) measurements during this period (section 2.2) benefit our assessment of the effectiveness of satellite data assimilation.

The results are presented in the following order: We first show the differences between our a posteriori results and those produced by the free-running modeling system. These include the changes in boundary condition model O_3 (section 3.1), in U.S. NO_x emission inputs along with the indication of urban emission trends and the impact of wildfires on anomalous high NO_x emissions in remote regions (section 3.2), and the resulting changes in the regional-modeled O_3 distributions (section 3.3). Cross validation is conducted to evaluate the effectiveness of the assimilation. Next, we use the surface background O_3 with satellite observation constraints to interpret the observed surface O_3 exceedances in multiple California air basins and Nevada (section 3.4). Finally, we suggest the future directions for modeling source attribution and satellite chemical data assimilation, as well as the development of future observing system (section 4).

2. Methods

2.1. Multi-scale Modeling System and the "A Priori"

We simulate air quality in California and Nevada from 15 June to 14 July 2008 using the regional Sulfur Transport and dEposition Model (STEM) on a $12 \times 12\,km^2$ Lambert conformal conic grid with 32 vertical layers in the troposphere [*Huang et al*., 2010, 2013]. The STEM simulations were driven by the meteorological fields modeled by the Advanced Research Weather Research and Forecasting (WRF-ARW) model [*Skamarock et al*., 2008] version 3.5, configured similarly to those in *Huang et al*. [2013]. The top and lateral chemical boundary conditions were downscaled from hourly output of the global Goddard Earth Observing System–Chemistry model (GEOS-Chem model) (http://geos-chem.org/; http://acmg.seas.harvard.edu/geos/geos_chem_narrative.html, and the references therein) adjoint version 34 [*Henze et al*., 2007] (http://wiki.seas.harvard.edu/geos-chem/index.php/GEOS-Chem_Adjoint_v34) on a 2° latitude × 2.5° longitude horizontal resolution grid and 47 vertical layers (up to 0.01 hPa) in the atmosphere (surface to ~100 hPa were simulated in the lowest 35 layers). The free-running GEOS-Chem simulation, defined as case GC_F_BASE (Table 1, together with the definitions of all model cases), used the similar key inputs to those used in *Bowman and Henze* [2012], spinning-up from the previous year.

The a priori anthropogenic emissions in STEM simulations came from the 2005 National Emission Inventory (NEI 05), and the emissions of several key gaseous species (sulfur dioxide, nonmethane volatile organic compounds (NMVOCs), NO_x, and carbon monoxide (CO)) were constantly scaled based on EPA-reported emission trends (http://www.epa.gov/ttnchie1/trends/). Biogenic emissions were generated by Model of Emissions of Gases and Aerosols from Nature version 2.0 [*Guenther et al*., 2006], driven by our WRF-simulated meteorology. We use biomass-burning emissions from the daily Quick Fire Emission Dataset version 2.4 (QFED, data received in December 2013) (A. S. Darmenov and A. da Silva, The Quick Fire Emissions Dataset (QFED): Documentation of versions 2.1, 2.2 and 2.4., Vol. 38, Technical report series on global modeling and data assimilation, NASA/TM-2015-104606, edited by R. D. Koster, in preparation, 2015). The QFED product was developed on 0.1°×0.1° horizontal resolution using a "top-down" approach,

in which the amount of combusted biomass was derived from the fire radiative power and wildfire locations observed by the Moderate Resolution Imaging Spectroradiometer instrument, and species-specific emission factors were applied to generate the fire emissions. Previous studies on Canadian and Saharan biomass-burning regions indicate higher QFED aerosol emissions than some other emission estimates, which may be associated with positive biases [e.g., *Bian et al*., 2013; *Zhang et al*., 2014].

In an additional simulation, we estimate background O_3 by zeroing out the anthropogenic emissions in STEM. The free-running base and background STEM simulations are defined as cases STEM_F_BASE and STEM_F_BKG, respectively. Slightly different from the method in *Lapina et al*. [2014], U.S. anthropogenic emissions in the boundary condition model (GEOS-Chem) simulation were not turned off in case STEM_F_BKG, as we assume that boundary condition O_3 concentrations in the eastern Pacific were mostly affected by "background" sources. This assumption is verified by quantifying the contributions of U.S. anthropogenic emissions to O_3 along the STEM western boundary in the eastern Pacific, based on the differences between cases STEM_F_BASE and STEM_F_BKG. Results indicated that during this period, the recirculated U.S. anthropogenic pollution only negligibly (i.e., $<6\%$) contributed to the total O_3 at any point along this boundary.

2.2. Observations

The level 2 (L2) O_3 profiles version 4 measured during both day and nighttimes from the Aura-Tropospheric Emission Spectrometer (TES) instrument [*Beer*, 2006] (http://tes.jpl.nasa.gov) were assimilated into the global GEOS-Chem model. Compared to the tropospheric O_3 profiles from other satellite instruments, TES O_3, in general, show larger degree of freedom for signal (~2.0) [e.g., *Zhang et al*., 2010], the trace of the averaging kernel matrix, which represents the sensitivity of the retrieved state to the true state [*Rodgers*, 2000]. TES O_3 retrievals generally have strong sensitivity to the free troposphere and show $<15\%$ positive biases over lidar and ozonesonde profiles in previous validation studies [*Nassar et al*., 2008; *Richards et al*., 2008; *Boxe et al*., 2010; *Verstraeten et al*., 2013]. Using different methods, earlier versions of TES O_3 profiles have been assimilated into several global models [e.g., *Parrington et al*., 2008, 2009; *Pierce et al*., 2009; *Singh et al*., 2011a, 2011b; *Miyazaki et al*., 2012], including older versions of GEOS-Chem. Many of these assimilation experiments showed enhanced analysis O_3 concentrations in the lower free troposphere, which better agreed with independent ozonesondes. The TES-constrained surface daytime (12:00–18:00 local times) background O_3 levels in the western U.S. are 1–9 ppbv higher than those based upon a GEOS-Chem free run [*Parrington et al*., 2009]. The grid-scale sampling density of the assimilated TES observations in this study is illustrated in Figure 1a. Polar orbit sampling resulted in larger density in high-latitude regions. Benefiting from the "step and stare" special observations (http://tes.jpl.nasa.gov/visualization/l2plots/) that supported the ARCTAS and Oxidant and Particle Photochemical Processes campaigns, higher sampling densities are found in Asia, the Pacific, and some western U.S. states.

Nitrogen dioxide (NO_2) tropospheric column measurements taken at early afternoon local times by the Aura-Ozone Monitoring Instrument (OMI) [*Levelt et al*., 2006] were assimilated into the regional STEM model, and the version 2.0 product developed by the Royal Netherlands Meteorological Institute was used [*Boersma et al*., 2011a, 2011b]. OMI NO_2 has recently been assimilated into STEM during the California Research at the Nexus of Air Quality and Climate Change field campaign in May 2010 [*Huang et al*., 2014] to generate grid-specific a posteriori NO_x emissions and improve the modeled chemical fields over the western U.S. We use a similar setup in this study. The grid-scale sampling densities of the assimilated OMI observations indicate higher values in central and southern California in this month (Figure 1b).

Different types of in situ measurements over three dimensions are used as independent observations to assess the effectiveness of the assimilation. They include (1) electrochemical cell ozonesondes [*Thompson et al*., 2011] launched at Trinidad Head (THD; 40.8°N, 124.2°W; location denoted in Figure 1d) within the Arctic Intensive Ozonesonde Network Study protocol (http://croc.gsfc.nasa.gov/arcions/). THD is a Northern California coastal site designed to characterize the air masses entering the U.S. [*Oltmans et al*., 2008]. These profiles on 8 days in June and 12 days in July measured within 11:00–14:00 Pacific daylight time (18:00–21:00 UTC) show strong O_3 variability in the free troposphere (Figures 1e and 1f). (2) Near-surface (i.e., <2 km, above ground (agl)) O_3, NO_2, and total reactive nitrogen (NO_y) observations collected during six NASA DC-8 flights (Figure 1g) over various locations in the eastern Pacific and California (on 18, 20, 22, 24, and 26 June and 13 July 2008, flight paths on individual days shown in Figure 2a), mostly during the daytimes. The 1 min merged data

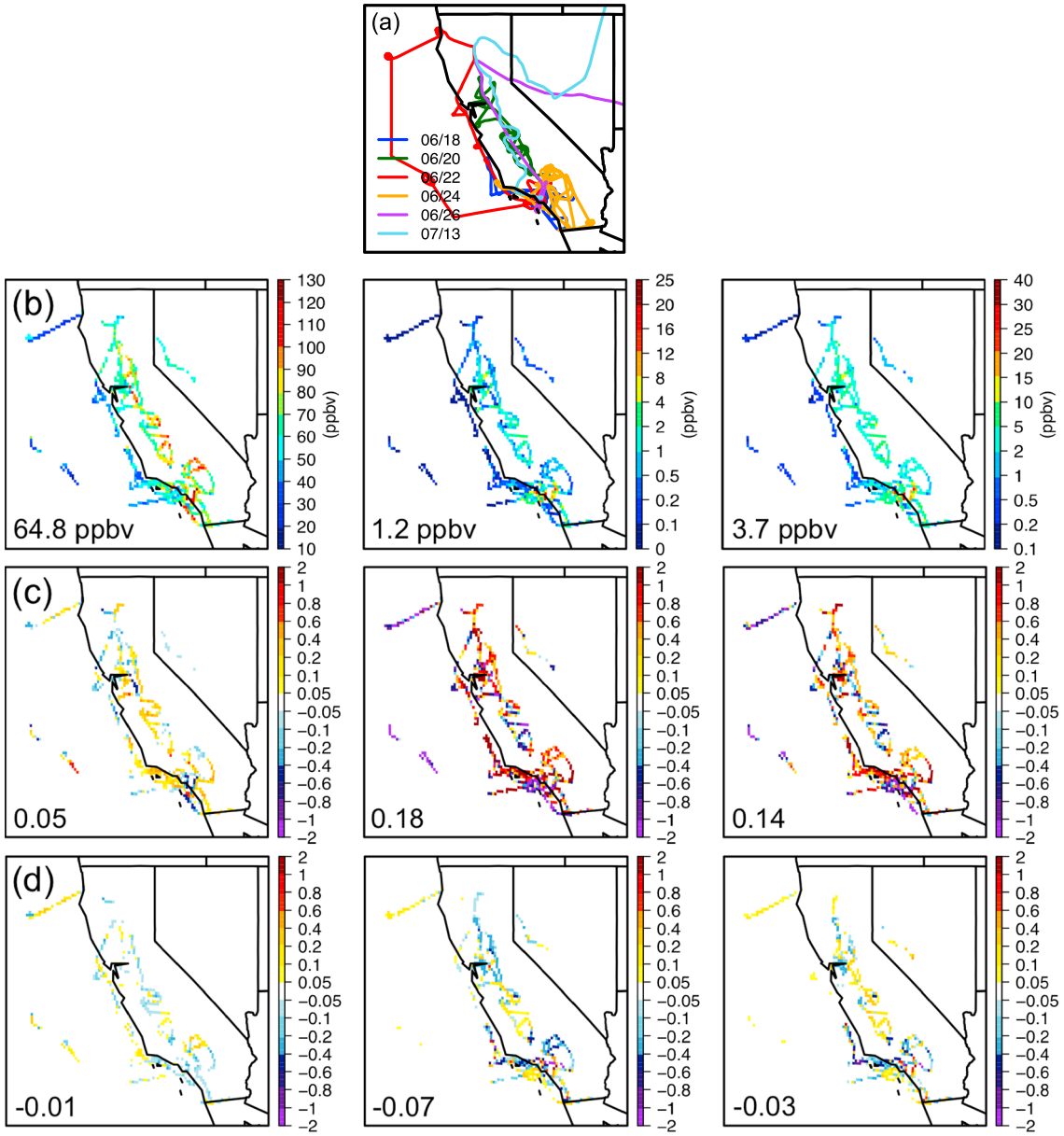

Figure 2. (a) DC-8 flight paths on 6 days during the studied period. (b–d) Evaluation of STEM-modeled near-surface (left column) O_3, (middle column) NO_2, and (right column) NO_y, along the six DC-8 flight paths, gridded to STEM resolution. Figure 2b shows the observed fields. Figure 2c shows the fractional bias ($2 \times$ (modeled − observed)/(modeled + observed), unitless) in case STEM_F_BASE, and Figure 2d shows the differences in fractional error ($2 \times |$modeled − observed$|$/(modeled + observed), unitless) between cases STEM_TO_BASE and STEM_F_BASE. Domain-mean values are indicated at the bottom left corner of each panel in Figures 2b–2d. The assimilation reduced domain-wide mean biases from 3.89 to 1.53 ppbv, 0.32 to −0.26 ppbv, and 0.71 to 0.32 ppbv, for O_3, NO_2, and NO_y, respectively.

were used as they have a closer spatial resolution to STEM's considering that the DC-8 aircraft has a top speed of ~14 km/min. Ozone and NO_y were measured by National Center for Atmospheric Research (NCAR)'s four-channel chemiluminescence instrument [*Weinheimer et al.*, 1993, 1994] (https://cloud1.arc.nasa.gov/arctas/docs/instruments/NOxyO3.pdf). The NO_2 measurements were made by two teams using the methods of thermal-dissociation laser-induced fluorescence [*Day et al.*, 2002] and chemiluminescence detection with photolytic conversion [*Weinheimer et al.*, 1993, 1994], respectively. We calculated the averages of the two sets of measurements for model evaluation. (3) Hourly O_3 from U.S. EPA Air Quality System (AQS) and Clean Air Status and Trends Network (CASTNET) surface sites (Figure 1h), measured by the ultraviolet absorbance method [*Office of Air Quality Planning and Standards*, 2008; *Clean Air Status and Trends Network*, 2009]. Both

the aircraft and surface O_3 observations show expanded areas of exceedances near the surface in California (Figures 1g and 1h).

2.3. Satellite Chemical Data Assimilation

Assimilation was applied sequentially in global and regional models to constrain the contributions to O_3 from nonlocal and local sources, respectively (Figure 1). The TES O_3 profiles were first assimilated into GEOS-Chem using the three-dimensional variational (3D-Var) approach [*Singh et al*., 2011a, 2011b], provided by GEOS-Chem Multi-mission Observation Operator (M_2O_2) system (http://wiki.seas.harvard.edu/geos-chem/index.php/Multi-mission_Observation_Operator_%28M2O2%29, and the references therein), a research task under NASA's Advanced Collaborative Connections for Earth System Science program, which aims to provide a mission-generic data assimilation capability for the GEOS-Chem adjoint model community (case GC_T_BASE; Table 1). We conducted a sensitivity test, in which the TES retrievals were multiplied by 0.85 to correct the known biases reported in literature (case GC_ScaleT_BASE). The a posteriori O_3 fields from both GC_T_BASE and GC_ScaleT_BASE cases were evaluated against the THD ozonesondes. The GC_T_BASE case shows better agreement with THD ozonesondes in the free troposphere at 400–900 hPa and therefore was selected for the follow-on analysis. These results are consistent with those in *Miyazaki et al*. [2012], who explored the impact of bias correction on the assimilation of TES O_3 into a different global model and concluded that applying constant scaling factors can improve the a posteriori only over certain regions. Then, using the TES-constrained boundary conditions extracted from case GC_T_BASE, STEM simulations were conducted using the a priori emission inputs (case STEM_T_BASE) and those constrained by OMI NO_2 tropospheric columns using the four-dimensional variational (4D-Var) approach [*Chai et al*., 2009; *Huang et al*., 2014]. The 4D-Var regional assimilation generated grid-specific a posteriori NO_x emissions. The same scaling factors were applied to NMVOCs, which are also important O_3 precursors. This is consistent with (1) the conclusions by *McDonald et al*. [2013], who indicated near-constant NO_x/NMVOC emission ratios in recent years over regions affected predominantly by mobile sources (e.g., urban areas); (2) the suggestions in the EPA-reported nationwide emission trends that relative changes of NO_x and NMVOC emissions during 2005–2008 are similar (i.e., ~10% decreases); and (3) the assumption that NO_x and NMVOC emissions from biomass burning are correlated. Similar coscaling methods have been used between CO and NMVOCs emissions [e.g., *Brioude et al*., 2013]. The resulting NO_2, NO_y, and O_3 fields were cross validated with available surface and aircraft in situ measurements. We define the base STEM simulation with OMI constraints as case STEM_TO_BASE (Table 1).

Two additional simulations were conducted to calculate the background O_3 with the TES O_3 or/and OMI NO_2 constraints. In case STEM_T_BKG, we used the same inputs as those in case STEM_F_BKG, except the TES-constrained boundary conditions. Further, in case STEM_TO_BKG, we used the same inputs as those in case STEM_T_BKG, except that we scaled the U.S. biomass-burning emissions only in the grids where the a priori QFED wildfire emissions are nonzero (mostly in remote regions), using the scaling factors generated from the regional assimilation. This method assumes that the regional assimilation identically adjusted biomass burning and anthropogenic emissions in these grids.

3. Results and Discussion

3.1. Ozone Improvement in TES-Constrained Boundary Condition Model

We quantify the changes in GEOS-Chem-modeled O_3 from the assimilation of TES O_3. We focus on the GEOS-Chem O_3 at altitudes between 700 hPa and 900 hPa in the eastern Pacific (latitude/longitude ranges of 30–50°N/140–120°W), as multiple studies have indicated that air masses at ~1–4 km in the eastern Pacific can impact inland near surface O_3 at later times in California [e.g., *Huang et al*., 2010; *Parrish et al*., 2010; *Yates et al*., 2014]. The a posteriori O_3 fields indicate domain-wide mean of 45.3 ppbv, ranging from $<$40 ppbv in the northeastern Pacific to $>$50 ppbv near shore and inland (Figure 3b). The posteriori enhanced the a priori by ~6 ppbv in average, increasing with latitude (Figures 3a–3c).

Ozone fields in GC_F_BASE and GC_T_BASE cases were compared against ozonesondes launched at THD. The vertical distributions of observed and GEOS-Chem O_3 in June and July 2008 are shown in Figures 3e–3f. The assimilation enhanced GEOS-Chem O_3 by 7.3 ppbv (16.3%) at 400–900 hPa, which reduced the biases from $-$11.5 ppbv ($-$20.3%) to $-$4.2 ppbv ($-$7.4%). We further explored the observed and GEOS-Chem O_3

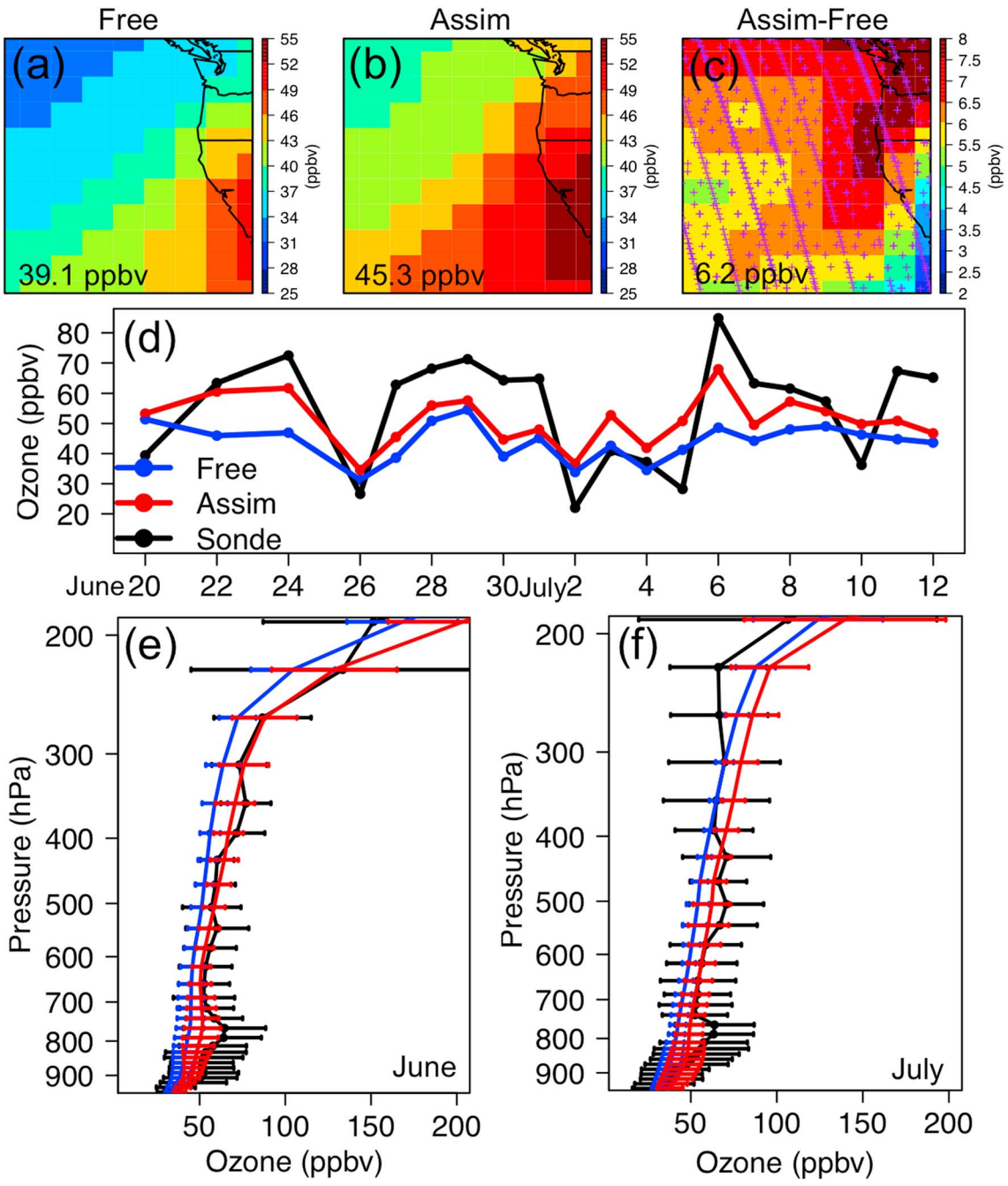

Figure 3. Period-mean O_3 in case (a) GC_F_BASE, (b) GC_T_BASE, and (c) the differences between Figures 3a and 3b with the TES sampling locations overlaid as purple plus signs. Figures 3a–3c were averaged from GEOS-Chem vertical level 7 to level 18 (~700–900 hPa in the eastern Pacific), and the domain-mean values are indicated at the bottom-left corner of each panel. (d) Time series of observed and GEOS-Chem-modeled O_3 at ~750 hPa at THD. The observations were calculated by binning the fine vertical resolution ozonesondes to GEOS-Chem level 16. Period-mean and standard deviation (horizontal lines) of observed and GEOS-Chem-modeled O_3 vertical profiles at THD in (e) June 2008 and (f) July 2008. The observations were calculated by binning the fine vertical resolution ozonesondes to each GEOS-Chem vertical layer.

temporal variability at ~750 hPa (Figure 3d). Multiple O_3 peaks (>60 ppbv) were observed possibly due to the impact of long-range transport of Asian pollution (22–25 June and 6–8 July) and U.S. biomass-burning emissions (22–25 June, 27 June to 1 July, and 11–12 July), according to previous findings [e.g., *Huang et al.*, 2010, 2013; *Jaffe et al.*, 2013]. The assimilated O_3 fields were enhanced by 1.9–19.3 ppbv relative to the free-running GEOS-Chem, with the period mean of 7.0 ppbv (15.8%). Although the assimilated fields are in better agreement with ozonesondes, there still remains a −3.9 ppbv (−7.0%) negative biases, and the O_3

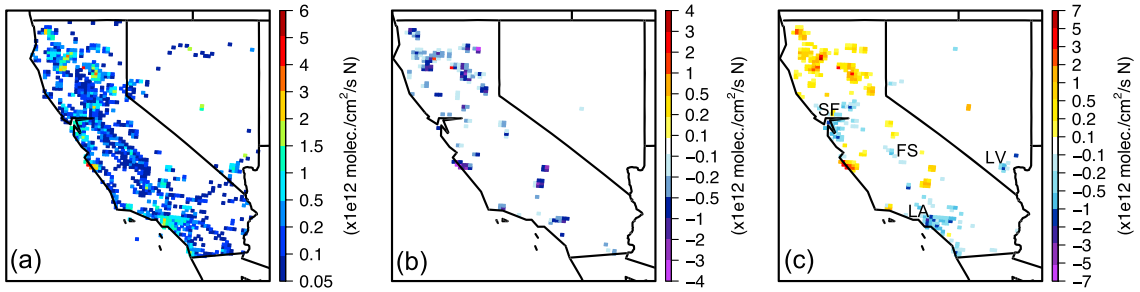

Figure 4. (a) A posteriori period-mean NO_x emissions from all source sectors from this study for summer 2008. (b) Differences of NO_x emissions in nonzero wildfire emission grids: a posteriori-a priori. (c) Differences of NO_x emissions: a posteriori (this study)—(NEI 05 + nonfire natural emissions, as a proxy to the 2005 conditions). Locations of several urban areas discussed in section 3.2 are denoted.

variability (standard deviation) is underestimated by a factor of 2. The most significant improvement of >15 ppbv occurred during the previously reported [*Huang et al*., 2010, 2013] (https://cloud1.arc.nasa.gov/arctas/flightDocs.php) strong trans-Pacific anthropogenic and wildfire pollution transport periods (i.e., 22/24 June and 6 July).

3.2. NO_x Emission Changes by Assimilating OMI NO_2

Over the California-Nevada domain, the assimilation of OMI NO_2 columns generated NO_x emission a posteriori of 0.4 Tg N/yr (Figure 4a). Compared to the sum of original NEI 05 and natural emissions, the a posteriori is 37% lower in the model grids that had nonzero monthly-mean biomass-burning NO_x emissions and 25% lower in the rest of the grids. Cross validation of the NO_2 and NO_y fields against aircraft measurements suggests an overall improvement: The mean fractional bias (i.e., $2\times$(modeled − observed)/(modeled + observed), unitless) for NO_2 and NO_y was reduced by ~39% and ~21%, respectively. The improvement is especially notable near the urban areas and its downwind regions, as well as the wildfire locations in Northern California (Figures 2b–2d).

The major sources of the positive biases in the daily-mean QFED wildfire emissions (Figure 4b) suggested by the assimilation results include (1) the omission of diurnal cycle. *Mu et al*. [2011] emphasized the importance of including diurnal cycle in biomass-burning emissions for accurately modeling CO concentrations. Diurnal cycle of biomass-burning emissions has been imposed in several modeling systems (e.g., GEOS-5) and would be also implemented into this modeling system in future and (2) the used emission factors from *Andreae and Merlet* [2001], dependent on the vegetation classifications. Our modeled CO near wildfires did not suggest such large positive bias in the QFED CO emissions (not shown in Figure) nor did another ARCTAS study by *Bian et al*. [2013]. The emission ratio between NO_x and CO in QFED is ~0.026 over the forest regions in Northern California and as high as ~0.056 in the Central Valley Savanna regions. These ratios are more than twice higher than what is indicated by ARCTAS aircraft observations: *Singh et al*. [2010] reported the enhancement ratio between NO_x (or NO_y) and CO to be <0.01 in fresh biomass-burning plumes. Therefore, the NO_x emission factors used for producing QFED emissions are likely unrealistic for this case. Indeed, natural variation of emission factors has been known to be one of the major sources of uncertainty in biomass-burning emission estimates [*van Leeuwen and van der Werf*, 2011]. However, our top-down approach over the wildfire-impacted regions may be complicated by the less understood flux uncertainties and higher uncertainties in OMI's air mass factors [*Bousserez*, 2014] and averaging kernel vectors propagated from those in the Tropospheric Model 4 NO_2 a priori used in the vertical column retrievals. Despite the positive biases in QFED emissions, the a posteriori estimates show anomalously high NO_x emissions in summer 2008 from wildfire emissions in Northern California and the Central Valley (Figure 4c), which can contribute to higher background O_3 than in 2005.

The ~25% reduction of NO_x emissions in nonfire grids, mainly from the anthropogenic emission sources, suggests that the NEI 05 NO_x emission estimates did not well represent the actual emissions during the studied period. Significant reductions are found over several key urban regions (Figure 4c): Las Vegas (LV 36.2°N, 115.2°W; −38.9%), San Francisco (SF; 37.6°N, 122.0°W; −45.5%), and Los Angeles (LA; 34.0°N, 117.9°W; −32.4%). These reductions are stronger than the Central Valley urban regions such as Fresno (FS 36.7°N, 119.75°W; −14.6%). These reductions can be partially due to the effective emission controlling strategies and the recent

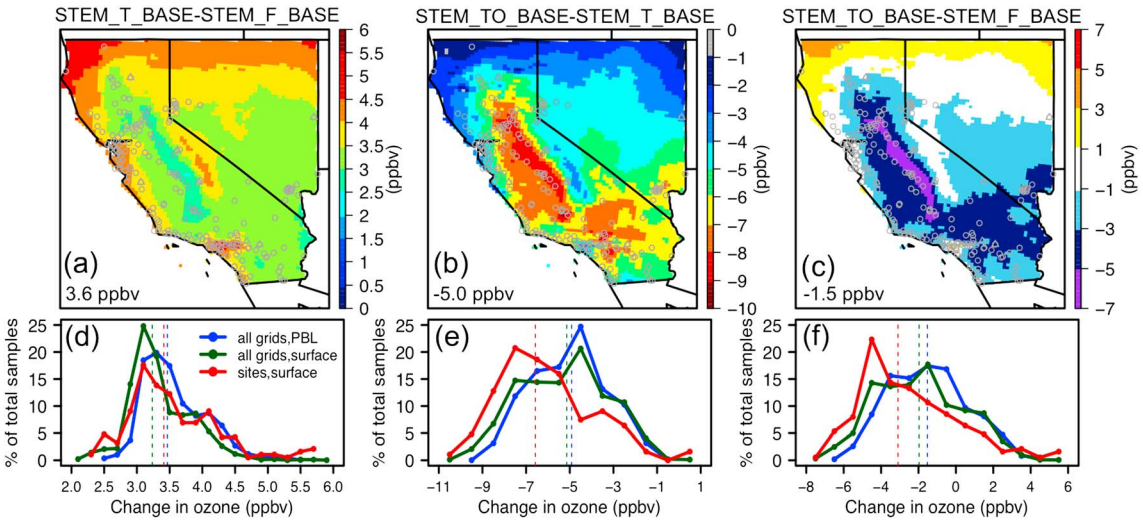

Figure 5. Changes in STEM-modeled daytime total O_3 between various cases: (a and d) STEM_T_BASE-STEM_F-BASE, indicating the differences made by using TES-constrained GEOS-Chem boundary conditions; (b and e) STEM_TO_BASE-STEM_T-BASE, indicating the differences made by constraining U.S. emissions with OMI; and (c and f) STEM_TO_BASE-STEM_F-BASE, indicating the net effects of integrating both TES and OMI measurements. Figures 5a–5c illustrate the near-surface O_3 differences (i.e., averaged from the model surface to ~2 km agl), and the domain-mean values are indicated at the bottom left corner of each panel. Figures 5d–5f show the histograms of O_3 differences in all grids near the surface (blue), at the surface grids (dark green), and only sampled at the surface monitoring sites (red). The vertical dash lines indicate the median values for each case.

economic recession, as discussed in previous observation-based and model-based studies that found region-dependent declining trends in NO_x concentrations and emissions in California since 2005 [e.g., *Russell et al.*, 2010, 2012; *Huang et al.*, 2014]. A possible additional reason is that the NEI 05 NO_x emission estimates have spatially and temporally varying uncertainties for the base year of 2005; e.g., *Lamsal et al.* [2014] showed that in 2005, the U.S. NO_x emissions in NEI 05 was higher than their OMI-constrained emission estimate during summertime but is opposite for springtime. Their annual mean bottom-up and top-down estimates for 2005 are close over the U.S. due to compensation of positive and negative differences found on small scales, but discussions focusing on California-Nevada regions are lacking in their study. A separate study using our assimilation system that explores NO_x emissions in the base year of 2005 can help prioritize these two reasons, and routinely taken in situ measurements associated with low uncertainties are favored for the purpose of cross validation. It is worth exploring better modeling and assimilation setup (e.g., alternative WRF configurations especially over the areas with complex terrains and more experiments on the length of assimilation window considering the variable NO_x lifetimes).

3.3. Near-Surface O_3 Changes From the Multi-scale Assimilation

Figures 5a–5c show that near-surface daytime (i.e., 08:00–19:00 local standard time, $<$~2 km agl) O_3 increased by ~4 ppbv in response to the changes in the GEOS-Chem boundary conditions, with the largest changes (4–6 ppbv) occurring in the high-elevation areas (i.e., terrain heights of 1–3 km) in Northern California and the Sierra-Nevada Mountain region and the minimum values (~2 ppbv) in the Central Valley. The spatial patterns of these changes are similar to those in GEOS-Chem in the free troposphere but are ~1–2 ppbv smaller in magnitude. *Steiner et al.* [2006] used the Community Multiscale Air Quality (CMAQ) regional model at 4 km horizontal resolution over a smaller domain centered in the SF Bay area to study the sensitivity of O_3 chemistry in Northern-Central California to western boundary conditions in summer 2000. They showed that the changes in O_3 chemical boundary conditions from constant 30 ppbv to 40 ppbv, along with the enhancement in CO and methane boundary conditions, led to increases in transported O_3 to California as well as modified local chemical production/loss. They reported 4–7 ppbv of O_3 increases in the SF-Monterey Bay areas but $<$3 ppbv in the Central Valley, as a result of the different net changes in transported and chemical production/loss rates. Our sensitivities indicate similar decreasing spatial gradient from the ocean in both SF and LA coastal urban regions, also reflecting fast chemistry over the high-emission regions (e.g., hydroxyl radical (OH) mixing ratios are up to 10 times higher than in the

Journal of Geophysical Research: Atmospheres

10.1002/2014JD022993

Table 2. Domain Mean ± Standard Deviation of Observed and STEM-Modeled Total and Background MDA8 O_3 at Surface Sites in California and Nevada[a]

	Total O_3 (ppbv)				Background O_3 (ppbv)			Background/Total O_3 (%)		
	Observations at Surface Sites	STEM_F_BASE	STEM_T_BASE	STEM_TO_BASE	STEM_F_BKG	STEM_T_BKG	STEM_TO_BKG	STEM_F_BKG/ STEM_F_BASE	STEM_T_BKG/ STEM_T_BASE	STEM_TO_BKG/ STEM_TO_BASE
All surface data (in all model grids)		67.7 ± 13.5	71.0 ± 13.3	64.3 ± 11.0	50.7 ± 6.2	54.0 ± 5.8	48.3 ± 3.9	76.3 ± 9.2	77.4 ± 9.3	76.7 ± 10.6
All surface data (at sites)	59.6 ± 16.6	75.9 ± 14.2 (*0.26*)	79.4 ± 14.1 (*0.31*)	71.2 ± 12.2 (*0.22*)	53.3 ± 5.5	56.4 ± 5.2	48.9 ± 3.6	72.0 ± 10.8	72.8 ± 10.9	69.6 ± 11.4
Observed >60 ppbv	74.4 ± 8.2	84.4 ± 12.9 (*0.16*)	87.8 ± 12.9 *(0.18)*	78.8 ± 11.1 (*0.11*)	58.5 ± 9.3	61.3 ± 9.2	52.3 ± 7.2	70.3 ± 11.2	70.8 ± 11.1	67.4 ± 11.5
Observed >65 ppbv	78.2 ± 7.2	87.9 ± 12.8 (*0.15*)	91.2 ± 12.7 (*0.18*)	81.4 ± 11.0 (*0.10*)	61.1 ± 11.2	63.9 ± 11.1	53.7 ± 8.2	70.4 ± 12.2	70.9 ± 12.1	67.0 ± 12.2
Observed >70 ppbv	81.9 ± 6.8	89.2 ± 13.8 (*0.13*)	92.6 ± 13.6 (*0.15*)	82.4 ± 11.7 (*0.10*)	62.7 ± 13.0	65.5 ± 12.7	54.6 ± 9.2	71.0 ± 13.2	71.5 ± 13.1	67.3 ± 12.9
Observed >75 ppbv	86.9 ± 5.9	92.8 ± 11.8 (*0.11*)	96.2 ± 11.1 (*0.13*)	86.0 ± 11.1 (*0.09*)	64.7 ± 12.8	67.4 ± 12.5	56.5 ± 11.1	70.2 ± 12.8	70.6 ± 12.7	66.4 ± 12.7

[a]For the "STEM_*_BASE" simulations, we calculated the mean fractional error (unitless, *italic*).

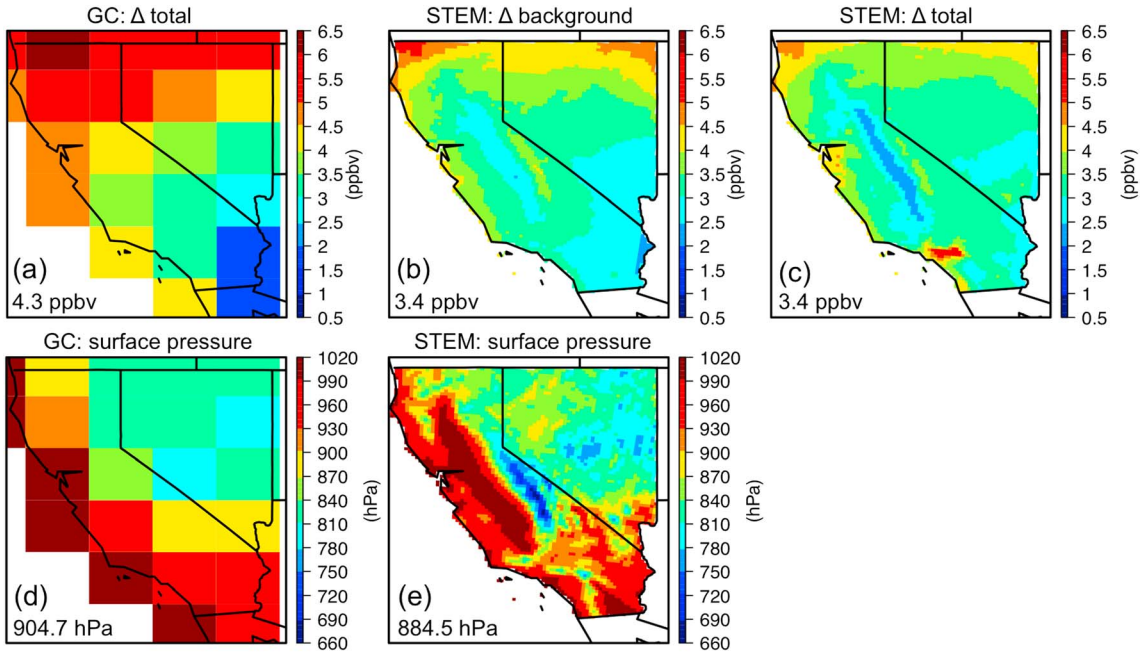

Figure 6. The differences of daytime surface O_3 between various cases: (a) GC_T_BASE-GC_F_BASE, (b) STEM_T_BKG-STEM_F_BKG, (c) STEM_T_BASE-STEM_F_BASE. Period-mean daytime surface pressure from (d) GEOS-5/Chem and (e) WRF-STEM modeling systems. Domain-mean values are indicated at the bottom left corner of each panel.

rural and remote areas inland). Near-surface O_3 dropped by ~5 ppbv in response to the changes in U.S. emissions, most strongly in the Central Valley and in Southern California downwind of LA (>8 ppbv). The net changes of O_3 caused by updating both the boundary conditions and U.S. emissions indicate decreases of 3–7 ppbv in the Central Valley and Southern California, whereas increases of 1–5 ppbv in Northern California and Nevada, and no notable net changes are found in central Nevada and the Sierra-Nevada Mountain regions. These results indicate that the multi-scale assimilation repartitioned the contributions of O_3 from nonlocal and local sources in California and Nevada and redistributed modeled near-surface O_3 in these regions.

The a posteriori O_3 fields (in case STEM_TO_BASE) were cross validated against independent near-surface aircraft (Figures 2b–2d) and surface measurements (Table 2) during this period, showing overall improvement from the a priori: the mean fractional error (i.e., $2\times|\text{modeled}-\text{observed}|/(\text{modeled}+\text{observed})$, unitless) in modeled near-surface O_3 along flight paths and the daily maximum 8 h average (MDA8; the metric for U.S. O_3 primary standard) at surface monitoring sites were reduced by ~20% and ~18%, respectively. The most significant improvement occurred in the areas of frequent O_3 exceedances such as the Central Valley and Southern California. The assimilation hardly improved O_3 in the Bay area where O_3 exceedances were less frequently observed. Urban-scale modeling with better meteorological fields and NMVOC treatments (chemistry, total emission, and speciation) will be needed for better simulating O_3 in these regions.

We further explored the vertical and horizontal variability of the modeled near-surface O_3 changes in response to the changes in boundary conditions and regional emissions. Vertically, we compared O_3 changes at the surface and near the surface. Although surface and near-surface changes show similar spatial patterns, the modeled surface O_3 concentrations are more sensitive to changes in the U.S. emissions and less sensitive to the boundary conditions than near-surface O_3 concentrations. The differences can be as high as ~2 ppbv on grid scale but <0.5 ppbv in average domain wide (histograms in Figures 5d–5f). Horizontally, we compared the O_3 changes in all model surface grids and those sampled only at surface monitoring sites. The significantly different shapes of the histograms (Figures 5d–5f) in these comparisons indicate that the changes that occurred after the assimilation at existing surface sites did not well represent those that occurred in all grids, as also shown in Figures 5a–5c. What the surface sites do not cover include many rural and remote regions in Nevada and California. In general, the changes of modeled O_3 in these observation-unavailable grids are larger

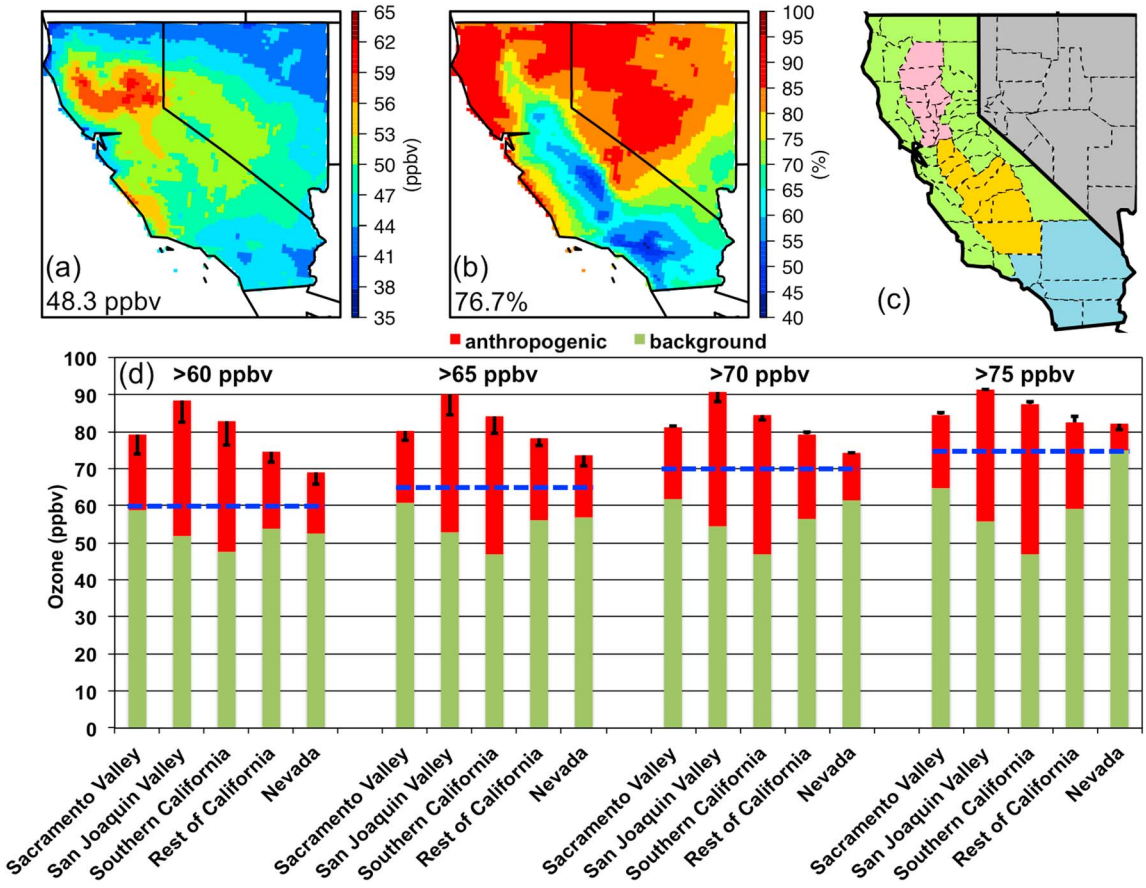

Figure 7. Modeled period-mean surface MDA8 background O_3 in (a) ppbv and (b) percentage contributions to the total O_3. Domain-mean values are indicated at the bottom left corner of each panel. (c) Various geographical regions are defined: (pink) Sacramento Valley, (orange) San Joaquin Valley, (blue) Southern California, (light green) rest of California, and (grey) Nevada. (d) Contributions of background O_3 (case STEM_TO_BKG, green bars) and local anthropogenic emissions (STEM_TO_BASE-STEM_TO_BKG, red bars) to the MDA8 exceedances at AQS and CASTNET surface sites in various regions defined in Figure 7c, using the current 75 ppbv and potential thresholds of 60, 65, and 70 ppbv denoted as horizontal blue dash lines. The error bars (in black line) indicate the observation-modeled discrepancies.

in response to updates in boundary conditions, and much smaller in response to changes in emissions, compared to those in the rest of the grids. Some near-surface locations where the strongest sensitivities to boundary conditions and/or U.S. emissions occurred were not sampled by the DC-8 aircraft either.

The impact of assimilating TES O_3 into GEOS-Chem on daytime surface O_3 in both models is also compared. The GEOS-Chem surface O_3 enhancements are ~1 ppbv higher than STEM's surface background and total O_3 responses to the updated GEOS-Chem boundary conditions (i.e., domain-wide mean of 4.3 ppbv and 3.4 ppbv, respectively; Figures 6a–6c). This can be mainly due to the different terrain heights (indicated by surface pressure from the two models shown in Figures 6d and 6e) and transport that are in part dependent on the model resolution. Whether or not there were TES data in the California-Nevada regions (STEM domain) can also be a factor. The changes in STEM surface total and background O_3 are different in spatial distributions despite their similar domain-wide mean values. This feature indicates that the inclusion of U.S. anthropogenic emissions modified the sensitivities of chemical production/loss in STEM on grid scale to the changes in chemical boundary conditions; i.e., the chemical coupling between transboundary and locally produced O_3 pollution is nonlinear. The surface O_3 enhancements in GEOS-Chem are ~1–2 ppbv smaller than those in the free troposphere shown in Figure 3c. This feature reflects the dilution that occurred as the air masses descended inland to affect the boundary layer air quality. Compared to results in *Parrington et al.* [2009], assimilation of TES O_3 in this study resulted in similar changes in GEOS-Chem surface O_3 in Northern California (~6 ppbv) but ~2–3 ppbv lower changes in Southern California and Nevada. This is mainly due to the different synoptic conditions in the two studied periods but is possibly also due to the selected versions of GEOS-Chem and TES O_3.

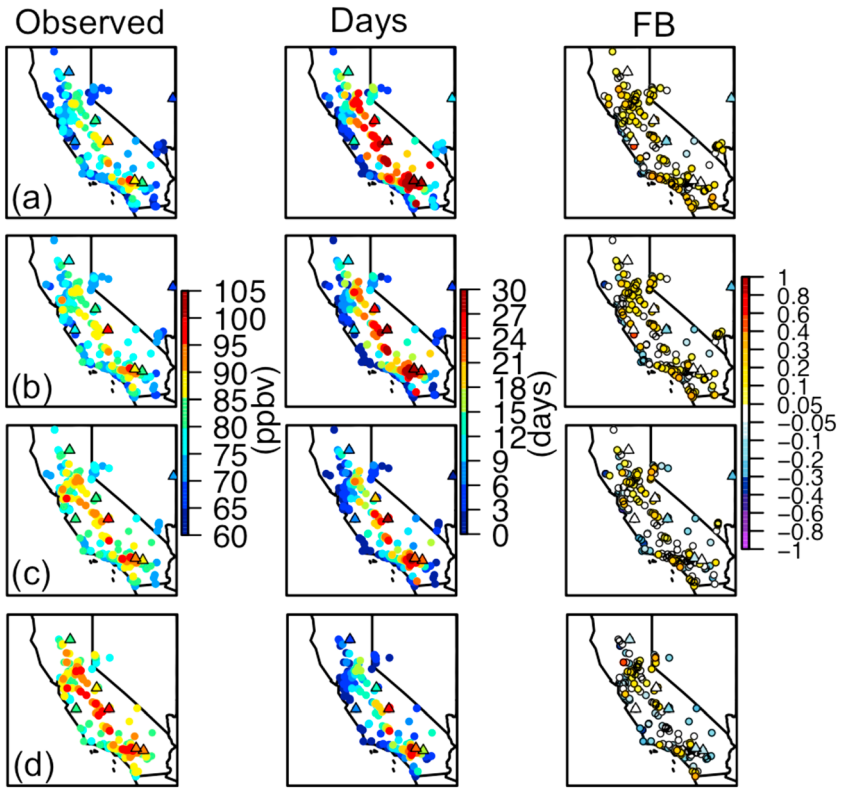

Figure 8. (column 1) The observed MDA8 at surface AQS (circles) and CASTNET (triangles) sites. (column 2) Number of days of O_3 exceedances at these sites. (column 3) Fractional bias (FB = 2 × (modeled − observed)/(modeled + observed)) of modeled MDA8 in case STEM_TO_BASE at the surface sites. The value at each surface site was averaged through the studied month for the days that the MDA8 exceeded (a) 60 ppbv, (b) 65 ppbv, (c) 70 ppbv, and (d) 75 ppbv. Statistics of the observed and modeled O_3 data are summarized in Table 2.

3.4. A Posteriori Background O_3 and Its Interpretation of Observed Surface O_3 Exceedances

The period-mean background MDA8 O_3 with observation constraints (in case STEM_TO_BKG) ranges spatially from 35 to 65 ppbv, with the domain-wide mean of ~48 ppbv (Figure 7a). The percentage contributions of these estimated background O_3 to the modeled total O_3 are 45–65% in the Central Valley and Southern California, and exceed 80% over the high-terrain remote regions in Northern California and the Sierra-Nevada Mountain, with the domain-wide mean of ~77% (Figure 7b). Although background O_3 averaged in all model grids is close to what is averaged only at the surface monitoring sites, the mean percentage contribution of background O_3 to total O_3 averaged in all grids is ~7% higher than what is calculated only at the surface sites (Table 2). This indicates that during this period, the existing surface monitoring network missed a large area mainly affected by background O_3. These include park regions where the O_3 pollution can be a concern for the tourists. Our background O_3 estimates fall in the range from 30 to >60 ppbv reported in previous studies by *Mueller and Mallard* [2011] and *Emery et al*. [2012] in the western U.S. during fire-affected periods in other years. The spatial patterns of our background O_3 percentage contributions to the total O_3 at surface sites show similar spatial gradients as those documented by U.S. EPA based on the Comprehensive Air-quality Model with extensions (CAMx) regional model calculations in 2007 in the same regions [*U.S. EPA*, 2014]. The contributions to the total O_3 in urban areas (mostly at low elevations) (40–60%) are smaller than those in the high-elevation rural and remote regions (>80%), which is consistent with the findings by *Lefohn et al*. [2014] that focus on the entire U.S.

We calculated the mean MDA8 total and background O_3 (in ppbv and % contributions to the total O_3) at each surface site on the days when the observed MDA8 was over a certain threshold (i.e., 60, 65, 70, 75 ppbv). Statistics of results at all surface sites are summarized in Table 2. It is shown that O_3 exceedances in case

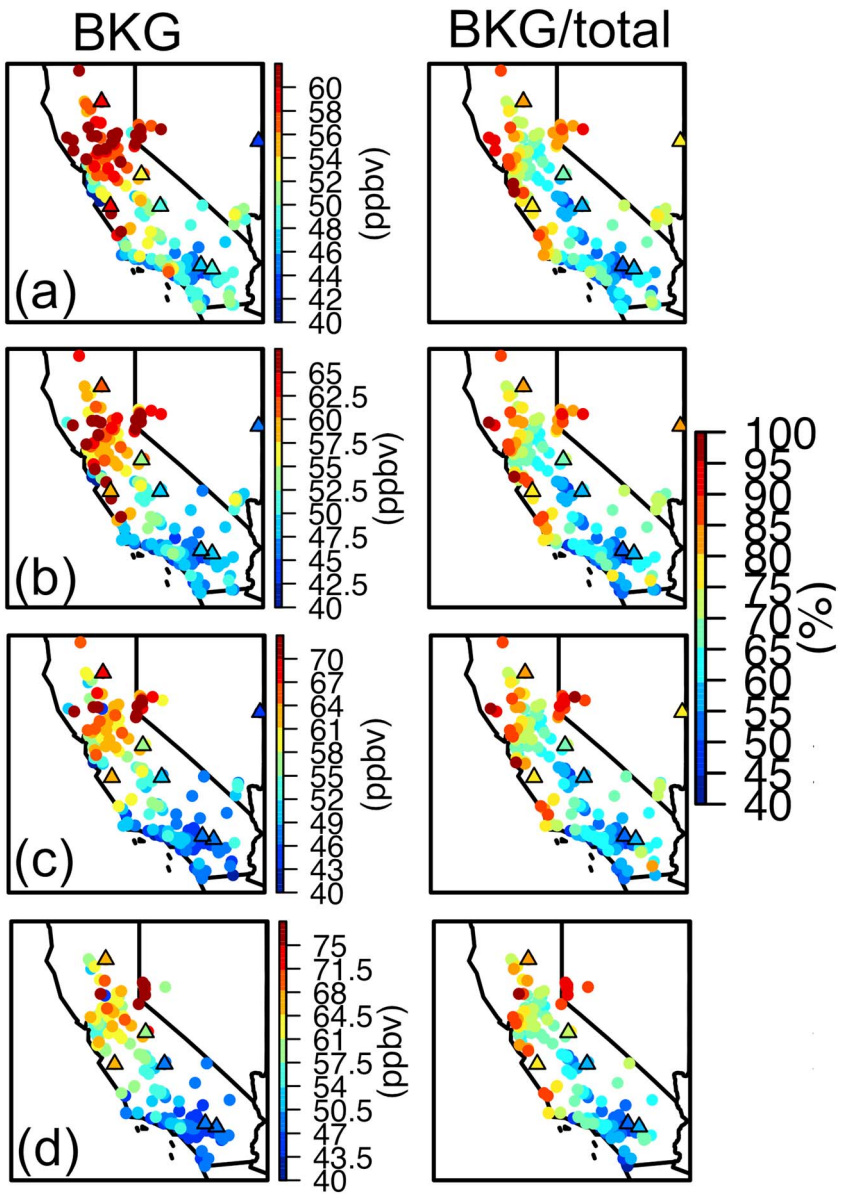

Figure 9. (left column) STEM estimated background MDA8 in case STEM_TO_BKG at the surface sites. (right column) Percentage contribution of background O_3 to the total O_3 (i.e., the ratio of STEM MDA8 between STEM_TO_BKG and STEM_TO_BASE). The value at each surface site was averaged through the studied month for the days that the MDA8 exceeded (a) 60 ppbv, (b) 65 ppbv, (c) 70 ppbv, and (d) 75 ppbv. Statistics of the modeled background O_3 data are summarized in Table 2.

STEM_TO_BASE are best modeled, i.e., associated with the smallest mean fractional errors. The mean and standard deviation of the absolute background O_3 increase with the threshold, i.e., ranging from 48.9 ppbv on all days to 56.5 ppbv on days when the observed O_3 exceeded 75 ppbv. However, the contributions to the modeled total O_3 are similar (~67%). This indicates that large-scale background O_3 is positively correlated with the total O_3. The a posteriori background O_3 at all these surface sites were ~5–8 ppbv lower than the a priori estimates, a net effect of the ~3 ppbv of enhancement by bringing up boundary conditions and the ~8–11 ppbv decreases by bringing down the U.S. wildfire emissions. These differences indicate the importance of incorporating observations to accurately attribute the observed O_3 exceedances in the western U.S.

The spatial distributions of the observed MDA8 on days exceeding the multiple thresholds are shown in Figure 8, along with model evaluation, and the corresponding background O_3 contributions are shown in Figure 9. The results are summarized as bar plots by various subregions including several California air basins and Nevada (Figure 7d). Highest total O_3 occurred in the San Joaquin Valley, followed by Southern California, Sacramento Valley, rest of California, and Nevada. In most of these subregions, the differences between the O_3 standard and the estimated background O_3 decrease as the threshold decreases, suggesting that more effective U.S. emission control actions will need to be taken in order to attain the lower potential O_3 standards (exception is found at Nevada sites for days exceeding 75 ppbv in which the fewest data samples were used in the calculation). Due to the strong wildfires impacts in this summer, background O_3 in California's Sacramento Valley is only $<$10 ppbv below each threshold. The background O_3 in Sacramento Valley is $>$5 ppbv higher than in San Joaquin Valley that also has low terrain heights but was away from the wildfires. Although the "rest of California" subregion was also less strongly affected by wildfires than Sacramento Valley, background O_3 there is 2–3 ppbv higher than in San Joaquin Valley, as it contains remote areas of complex terrain, which are more subject to the transported background O_3 impacts. The lowest background O_3 levels occurred in Southern California where larger anthropogenic O_3 would be possible (up to 20 ppbv) without exceeding the NAAQS.

4. Summary and Suggestions for Future Directions

This study integrates TES O_3 profiles and OMI tropospheric NO_2 columns into a multi-scale assimilation system composed of the global GEOS-Chem model and the regional STEM models, for better attributing the sources impacting western U.S. air quality. This system repartitioned and redistributed the contributions from nonlocal and local anthropogenic/wildfires sources to the modeled total and background O_3 in California and Nevada during the NASA ARCTAS field campaign period in summer 2008. We computed the mean observation-constrained surface background MDA8 O_3 to be ~48 ppbv in California and Nevada, which contributed to ~77% of the modeled total O_3. Due to the strong wildfire impacts during the studied period, the highest background O_3 occurred in California's Sacramento Valley, where it was $<$10 ppbv below the current and several proposed O_3 primary standards on the observed days of exceedance. Lowest background O_3 occurred in Southern California, and on observed days of O_3 exceedances, larger additional anthropogenic contributions (up to 20 ppbv) would be possible without exceeding the multiple thresholds.

We show that for all days and in all model grids, the observation-constrained background O_3 was 2.4 ppbv lower than the estimates from a free-running modeling system, as a result of a 3.3 ppbv increase in the nonlocal source contributions offset by a 5.7 ppbv of decrease in the local biomass-burning source contributions. The net differences are almost twice as large (i.e., 4.4 ppbv) if sampled only at the surface monitoring sites that do not cover many rural and remote regions in Nevada and California. In general, the changes of modeled O_3 in these observation-unavailable grids are larger in response to updates in boundary conditions, compared to those in the rest of the grids, whereas much smaller in response to changes in emissions. Therefore, there exists limitation in the current surface in situ network as certain regions that are sensitive to nonlocal sources and/or U.S. emissions are not included. In addition, GEOS-Chem O_3 in this study was evaluated only at one ozonesonde location in the western U.S., which indicated that the assimilation of TES observations improved the simulated contributions from transboundary pollution. Such evaluation can benefit from incorporating routine measurements of O_3 profiles overexpanded regions (e.g., surface lidar networks such as Tropospheric Ozone Lidar Network and Measurement of Ozone and Water Vapor on Airbus In-service Aircraft (MOZAIC)-like projects that take measurements on commercial aircraft). The NO_x and NO_y fields were only cross validated with independent aircraft measurements to indicate the improved contributions from U.S. emissions. However, aircraft measurements are limited in space and time. Most of the surface NO_2 measurements taken by chemiluminescence detection at U.S. monitoring stations with catalytic conversion on a molybdenum surface are known to be sensitive to some other NO_y species [e.g., *Dunlea et al.*, 2007]. The alternative photolytic conversion method avoids these positive biases [*Hall et al.*, 2012], and its broader application could benefit the evaluation of top-down NO_x emission estimates.

We recommend that in future, such multi-scale modeling and assimilation techniques to be extensively applied in chemical transport models. As shown by *Parrington et al.* [2008], assimilation of TES O_3 into different models can result in different a posteriori O_3, and therefore, multi-model assimilation and intercomparison should be encouraged for better assessing and reducing residual uncertainties. Currently, multiple global models already have satellite data assimilation capability, e.g., GEOS-Chem, Realtime Air Quality Modeling System (RAQMS) [*Pierce et al.*, 2007], and Global and regional Earth-system Monitoring using Satellite and in-situ data (GEMS)/Monitoring Atmospheric Composition and Climate project (MACC) [*Schere et al.*, 2012] (http://www.gmes-atmosphere.eu/documents/reports/), and they could serve as observation-constrained boundary conditions for regional models. The development and improvement in regional-scale assimilation capability should be strongly encouraged. Efforts could be made to increase the number of models that have the regional 4D-Var assimilation capability, to better understand the factors affecting the assimilation results in order to improve the similar assimilation methods, and to explore the alternative methods (e.g., see related discussions in *Singh et al.* [2011b], *Chai et al.* [2009], and *Huang et al.* [2014]).

We suggest similar source attribution analysis to be applied during extended periods and overexpanded regions; in that, a number of U.S. states are subject to periodically strong impacts of stratospheric intrusion and long-range transport of pollution from Asia and Europe [e.g., *Lin et al.*, 2012a, 2012b]. The extraregional pollution impacts can be seasonal and interannually variable [e.g., *TF HTAP*, 2010]; U.S. NO_x emission reductions occurred in various regions during the past decade, particularly from the megacities and power plants [e.g., *Parrish et al.*, 2011; *Duncan et al.*, 2013; *de Gouw et al.*, 2014]; certain U.S. emission sources may be missing or highly uncertain in bottom-up emission estimates but are detectable in space (e.g., flaring in North Dakota and Texas and biomass burning).

High-resolution regional assimilation would also benefit from the integration of newer and/or future satellite observations, preferably those with improved retrieval algorithms and/or better quantification of the retrieval uncertainties. Future satellite missions will routinely provide daytime measurements of O_3 and its key precursors with fine footprints; e.g., the TROPOspheric Monitoring Instrument (TROPOMI) on Sentinel-5 to be launched in 2015 [*Veefkind et al.*, 2012] and the geostationary Tropospheric Emissions: Monitoring of Pollution (TEMPO) to be launched in 2018–2019 [*Hilsenrath and Chance*, 2013] are designed to have footprint sizes of $\sim 7 \times 7\,km^2$ and $\sim 2 \times 5\,km^2$ (over California), respectively (http://www.knmi.nl/research/climate_observations/news/images/20110411_EGU_veefkind_poster_egu_tropomi.pdf; http://acmg.seas.harvard.edu/presentations/aqast/jun2014/Day1_AM/3-KChance-AQAST-17jun2014.pdf). Ozone retrievals have achieved higher sensitivity in the boundary layer; e.g., *Fu et al.* [2013] demonstrated the robustness of combining ultraviolet and infrared radiances from TES and OMI to obtain improved O_3 retrievals with stronger sensitivity in the troposphere including the boundary layer. Such techniques should also be applicable to newer instruments such as the Cross-track Infrared Sounder (CrIS) and Ozone Mapping and Profiler Suite (OMPS) instruments on the Suomi NPP satellite, as well as future satellite missions.

Furthermore, we suggest reducing uncertainties in the estimates of other background and total O_3 contributors, such as biogenic VOCs and lightning NO_x emissions. Although we focus on O_3 in this study, such multi-scale assimilation technique is applicable for studying other trace gases (e.g., CO) and aerosols. Constructing multi-scale multi-species chemical data assimilation system would be encouraged.

Acknowledgments

This work was mostly carried out at Jet Propulsion Laboratory, California Institute of Technology, under a contract with NASA, supported by the NASA Aura-TES project. We thank the Aura and ARCTAS science teams. G.R.C., D.K.H., and M.H. would like to acknowledge the NASA Air Quality Applied Sciences Team. The DC-8 aircraft measurements used in this study were made by A.J. Weinheimer (NCAR, O_3, and NO_{xy}) and R.C. Cohen (UC Berkeley, NO_2). We also acknowledge the computational resources at University of Iowa and at NASA Ames Research Center. We also acknowledge open access to the data and model used for this study, downloaded from the following:

- AQS: http://www.epa.gov/ttn/airs/airsaqs/detaildata
- CASTNET: http://epa.gov/castnet/javaweb/index.html
- DC-8: http://www-air.larc.nasa.gov/cgi-bin/arcstat-c
- OMI: http://www.temis.nl/airpollution/no2col/data/omi/data_v2/2008/
- TES: http://tes.jpl.nasa.gov/data/
- M2O2: http://wiki.seas.harvard.edu/geos-chem/index.php/Multi-mission_Observation_Operator_%28M2O2%29

- Ozonesondes: http://www.esrl.noaa.gov/gmd/dv/ftpdata.html

References

Ainsworth, E. A., C. R. Yendrek, S. Sitch, W. J. Collins, and L. D. Emberson (2012), The effect of tropospheric ozone on net primary productivity and implications for climate change, *Annu. Rev. Plant Biol.*, *63*, 637–661.

Ambrose, J., D. Reidmiller, and D. Jaffe (2011), Causes of high O_3 in the lower free troposphere over the Pacific Northwest as seen at the Mt. Bachelor Observatory, *Atmos. Environ.*, *45*(30), 5302–5315, doi:10.1016/j.atmosenv.2011.06.056.

Andreae, M. O., and P. Merlet (2001), Emission of trace gases and aerosols from biomass burning, *Global Biogeochem. Cycles*, *15*(4), 955–966, doi:10.1029/2000GB001382.

Anenberg, S. C., L. W. Horowitz, D. Q. Tong, and J. J. West (2010), An estimate of the global burden of anthropogenic ozone and fine particulate matter on premature human mortality using atmospheric modeling, *Environ. Health Perspect.*, *118*(9), 1189–1195.

Avnery, S., D. L. Mauzerall, J. Liu, and L. W. Horowitz (2011a), Global crop yield reductions due to surface ozone exposure: 1. Year 2000 crop production losses and economic damage, *Atmos. Environ.*, *45*, 2284–2296.

Avnery, S., D. L. Mauzerall, J. Liu, and L. W. Horowitz (2011b), Global crop yield reductions due to surface ozone exposure: 2. Year 2030 Potential crop production losses and economic damage under two scenarios of O_3 pollution, *Atmos. Environ.*, *45*, 2297–2309.

Avnery, S., D. L. Mauzerall, and A. M. Fiore (2013), Increasing global agricultural production by reducing ozone damages via methane emission controls and ozone resistant cultivar selection, *Global Change Biol.*, *19*, 1285–1299, doi:10.1111/gcb.12118.

Beer, R. (2006), TES on the Aura mission: Scientific objectives, measurements, and analysis overview, *IEEE Trans. Geosci. Remote Sens.*, *44*, 1102–1105.
Bian, H., et al. (2013), Source attributions of pollution to the Western Arctic during the NASA ARCTAS field campaign, *Atmos. Chem. Phys.*, *13*, 4707–4721, doi:10.5194/acp-13-4707-2013.
Boersma, K. F., R. Braak, and R. J. van der A (2011a), Dutch OMI NO_2 (DOMINO) data product v2.0 HE5 data file user manual. [Available at http://www.temis.nl/docs/OMI_NO2_HE5_2.0_2011.pdf.]
Boersma, K. F., et al. (2011b), An improved tropospheric NO_2 column retrieval algorithm for the Ozone Monitoring Instrument, *Atmos. Meas. Tech.*, *4*, 1905–1928.
Bousserez, N. (2014), Space-based retrieval of NO_2 over biomass burning regions: Quantifying and reducing uncertainties, *Atmos. Meas. Tech.*, *7*, 3431–3444, doi:10.5194/amt-7-3431-2014.
Bouttier, F., and P. Courtier (1999), Data assimilation concepts and methods. [Available at http://old.ecmwf.int/newsevents/training/rcourse_notes/DATA_ASSIMILATION/ASSIM_CONCEPTS/Assim_concepts.html.]
Bowman, K., and D. K. Henze (2012), Attribution of direct ozone radiative forcing to spatially resolved emissions, *Geophys. Res. Lett.*, *39*, L22704, doi:10.1029/2012GL053274.
Bowman, K. W., et al. (2013), Evaluation of ACCMIP outgoing longwave radiation from tropospheric ozone using TES satellite observations, *Atmos. Chem. Phys.*, *13*, 4057–4072, doi:10.5194/acp-13-4057-2013.
Boxe, C. S., et al. (2010), Validation of northern latitude Tropospheric Emission Spectrometer stare ozone profiles with ARCIONS sondes during ARCTAS: Sensitivity, bias and error analysis, *Atmos. Chem. Phys.*, *10*, 9901–9914.
Brioude, J., et al. (2013), Top-down estimate of surface flux in the Los Angeles Basin using a mesoscale inverse modeling technique: Assessing anthropogenic emissions of CO, NO_x and CO_2 and their impacts, *Atmos. Chem. Phys.*, *13*, 3661–3677.
Camalier, L., W. Cox, and P. Dolwick (2007), The effects of meteorology on ozone in urban areas and their use in assessing ozone trends, *Atmos. Environ.*, *41*, 7127–7137.
Carmichael, G. R., A. Sandu, T. Chai, D. N. Daescu, E. M. Constantinescu, and Y. Tang (2008), Predicting air quality: Improvements through advanced methods to integrate models and measurements, *J. Comput. Phys.*, *227*, 3540–3571, doi:10.1016/j.jcp.2007.02.024.
CASTNET (2009), Clean Air Status and Trends Network 2009 Annual Report. [Available at http://epa.gov/castnet/javaweb/docs/annual_report_2009.pdf.]
Chai, T., G. R. Carmichael, A. Sandu, Y. Tang, and D. N. Daescu (2006), Chemical data assimilation of Transport and Chemical Evolution over the Pacific (TRACE-P) aircraft measurements, *J. Geophys. Res.*, *111*, D02301, doi:10.1029/2005JD005883.
Chai, T., et al. (2007), Four-dimensional data assimilation experiments with ICARTT (International Consortium for Atmospheric Research on Transport and Transformation) ozone measurements, *J. Geophys. Res.*, *112*, D12S15, doi:10.1029/2006JD007763.
Chai, T., G. R. Carmichael, Y. Tang, A. Sandu, A. Heckel, A. Richter, and J. P. Burrows (2009), Regional NO_x emission inversion through a four-dimensional variational approach using SCIAMACHY tropospheric NO_2 column observations, *Atmos. Environ.*, *43*, 5046–5055.
Cooper, O., and J. Ziemke (2014), [Global Climate] Tropospheric Ozone [in "State of the Climate in 2013"], *Bull. Am. Meteorol. Soc.*, *95*(7), S42.
Cooper, O. R., et al. (2010), Increasing springtime ozone mixing ratios in the free troposphere over western North America, *Nature*, *463*, doi:10.1038/nature08708.
Cooper, O. R., et al. (2011), Measurement of western U.S. baseline ozone from the surface to the tropopause and assessment of downwind impact regions, *J. Geophys. Res.*, *116*, D00V03, doi:10.1029/2011JD016095.
Cooper, O. R., R. S. Gao, D. W. Tarasick, T. Leblanc, and C. Sweeney (2012), Long-term ozone trends at rural ozone monitoring sites across the United States, 1990–2010, *J. Geophys. Res.*, *117*, D22307, doi:10.1029/2012JD018261.
Cooper, O. R., et al. (2014), Global distribution and trends of tropospheric ozone: An observation-based review, *Elem. Sci. Anthropol.*, *2*, 000,029.
Day, D. A., P. J. Wooldridge, M. B. Dillon, J. A. Thornton, and R. C. Cohen (2002), A thermal dissociation laser-induced fluorescence instrument for in situ detection of NO_2, peroxy nitrates, alkyl nitrates, and HNO_3, *J. Geophys. Res.*, *107*(D5-6), 4046, doi:10.1029/2001JD000779.
de Gouw, J. A., D. D. Parrish, G. J. Frost, and M. Trainer (2014), Reduced emissions of CO_2, NO_x, and SO_2 from U.S. power plants owing to switch from coal to natural gas with combined cycle technology, *Earth's Future*, *2*, 75–82, doi:10.1002/2013EF000196.
Duncan, B. N., Y. Yoshida, B. de Foy, L. N. Lamsal, D. G. Streets, Z. Lu, K. E. Pickering, and N. A. Krotkov (2013), The observed response of Ozone Monitoring Instrument (OMI) NO_2 columns to NO_x emission controls on power plants in the United States: 2005–2011, *Atmos. Environ.*, *81*, 102–111, doi:10.1016/j.atmosenv.2013.08.068.
Dunlea, E. J., et al. (2007), Evaluation of nitrogen dioxide chemiluminescence monitors in a polluted urban environment, *Atmos. Chem. Phys.*, *7*, 2691–2704.
Emery, C., J. Jung, N. Downey, J. Johnson, M. Jimenez, G. Yarwood, and R. Morris (2012), Regional and global modeling estimates of policy relevant background ozone over the United States, *Atmos. Environ.*, *47*, 206–217.
Fiore, A. M., et al. (2009), Multimodel estimates of intercontinental source receptor relationships for ozone pollution, *J. Geophys. Res.*, *114*, D04301, doi:10.1029/2008JD010816.
Fiore, A. M., J. T. Oberman, M. Y. Lin, L. Zhang, O. E. Clifton, D. J. Jacob, V. Naik, L. W. Horowitz, J. P. Pinto, and G. P. Milly (2014), Estimating North American background ozone in U.S. surface air with two independent global models: Variability, uncertainties, and recommendations, *Atmos. Environ.*, *96*, 284–300, doi:10.1016/j.atmosenv.2014.07.045.
Fishman, J., K. M. Belina, and C. H. Encarnacion (2014), The St. Louis Ozone Gardens: Visualizing the impact of a changing atmosphere, *Bull. Am. Meteorol. Soc.*, 1171–1176, doi:10.1175/BAMS-D-13-00009.1.
Fu, D., J. R. Worden, X. Liu, S. S. Kulawik, K. W. Bowman, and V. Natraj (2013), Characterization of ozone profiles derived from Aura TES and OMI radiances, *Atmos. Chem. Phys.*, *13*, 3445–3462, doi:10.5194/acp-13-3445-2013.
Gratz, L. E., D. A. Jaffe, and J. R. Hee (2014), Causes of increasing ozone and decreasing carbon monoxide in springtime at the Mt. Bachelor Observatory from 2004 to 2013, *Atmos. Environ.*, doi:10.1016/j.atmosenv.2014.05.076.
Guenther, A., T. Karl, P. Harley, C. Wiedinmyer, P. I. Palmer, and C. Geron (2006), Estimates of global terrestrial isoprene emissions using MEGAN (Model of Emissions of Gases and Aerosols from Nature), *Atmos. Chem. Phys.*, *6*, 3181–3210, doi:10.5194/acp-6-3181-2006.
Hall, E., M. Beaver, R. W. Long, and R. W. Vanderpool (2012), EPA's reference and equivalent supporting NAAQS implementation through Methods Research Program: Research, development, and analysis, *Air Waste Manage. Assoc. Mag. Environ. Manage.*, *5*, 8–12.
Henze, D. K., A. Hakami, and J. H. Seinfeld (2007), Development of the adjoint of GEOS-Chem, *Atmos. Chem. Phys.*, *7*, 2413–2433, doi:10.5194/acp-7-2413-2007.
Hilsenrath, E., and K. Chance (2013), NASA ups the TEMPO on monitoring air pollution, *Earth Obs.*, *25*, 10–15.
Huang, M., et al. (2010), Impacts of transported background ozone on California air quality during the ARCTAS-CARB period – A multi-scale modeling study, *Atmos. Chem. Phys.*, *10*, 6947–6968, doi:10.5194/acp-10-6947-2010.
Huang, M., et al. (2013), Impacts of transported background pollutants on summertime western U.S. air quality: Model evaluation, sensitivity analysis and data assimilation, *Atmos. Chem. Phys.*, *13*, 359–391, doi:10.5194/acp-13-359-2013.

Huang, M., et al. (2014), Changes in nitrogen oxides emissions in California during 2005–2010 indicated from top-down and bottom-up emission estimates, *J. Geophys. Res. Atmos.*, *119*, 12,928–12,952, doi:10.1002/2014JD022268.

Jacob, D. J., et al. (2010), The Arctic Research of the Composition of the Troposphere from Aircraft and Satellites (ARCTAS) mission: Design, execution, and first results, *Atmos. Chem. Phys.*, *10*, 5191–5212, doi:10.5194/acp-10-5191-2010.

Jaffe, D. (2011), Relationship between surface and free tropospheric ozone in the western U.S, *Environ. Sci. Technol.*, *45*, 432–438, doi:10.1021/es1028102.

Jaffe, D. A., W. Hafner, D. Chand, A. Westerling, and D. Spracklen (2008), Influence of fires on O_3 concentrations in the western U.S, *Environ. Sci. Technol.*, *42*(16), 5885–5891, doi:10.1021/es800084k.

Jaffe, D. A., N. Wigder, N. Downey, G. Pfister, A. Boynard, and S. B. Reid (2013), Impact of wildfires on ozone exceptional events in the western U.S, *Environ. Sci. Technol.*, *47*, 11,065–11,072, doi:10.1021/es402164f.

Lamsal, L. N., et al. (2014), Evaluation of OMI operational standard NO_2 column retrievals using in situ and surface-based NO_2 observations, *Atmos. Chem. Phys.*, *14*, 11,587–11,609, doi:10.5194/acp-14-11587-2014.

Langford, A. O., J. Brioude, O. R. Cooper, C. J. Senff, R. J. Alvarez II, R. M. Hardesty, B. J. Johnson, and S. J. Oltmans (2011), Stratospheric influence on surface ozone in the Los Angeles area during late spring and early summer of 2010, *J. Geophys. Res.*, *117*, D00V06, doi:10.1029/2011JD016766.

Langford, A. O., et al. (2014), An overview of the 2013 Las Vegas Ozone Study (LVOS): Impact of stratospheric intrusions and long-range transport on surface air quality, *Atmos. Environ.*, doi:10.1016/j.atmosenv.2014.08.040.

Lapina, K., D. K. Henze, J. B. Milford, M. Huang, M. Lin, A. M. Fiore, G. Carmichael, G. G. Pfister, and K. Bowman (2014), Assessment of source contributions to seasonal vegetative exposure to ozone in the U.S, *J. Geophys. Res. Atmos.*, *119*, 324–340, doi:10.1002/2013JD020905.

Lefohn, A. S., C. Emery, D. Shadwick, H. Wernli, J. Jung, and S. J. Oltmans (2014), Estimates of background surface ozone concentrations in the United States based on model-derived source apportionment, *Atmos. Environ.*, *84*, 275–288, doi:10.1016/j.atmosenv.2013.11.033.

Levelt, P. F., G. H. J. van den Oord, M. R. Dobber, A. Malkki, H. Visser, J. de Vries, P. Stammes, J. O. V. Lundell, and H. Saari (2006), The Ozone Monitoring Instrument, *IEEE Trans. Geosci. Remote Sens.*, *44*(5), doi:10.1109/TGRS.2006.872333.

Lin, M., et al. (2012a), Transport of Asian ozone pollution into surface air over the western United States in spring, *J. Geophys. Res.*, *117*, D00V07, doi:10.1029/2011JD016961.

Lin, M., A. Fiore, O. R. Cooper, L. W. Horowitz, A. O. Langford, H. Levy II, B. J. Johnson, V. Naik, S. J. Oltmans, and C. J. Senff (2012b), Springtime high surface ozone events over the western United States: Quantifying the role of stratospheric intrusions, *J. Geophys. Res.*, *117*, D00V22, doi:10.1029/2012JD018151.

McCarthy, J. E. (2010), Ozone air quality standards: EPA's proposed January 2010 revision. [Available at http://www.fas.org/sgp/crs/misc/R41062.pdf.]

McDonald, B. C., T. R. Dallmann, E. W. Martin, and R. A. Harley (2012), Long-term trends in nitrogen oxide emissions from motor vehicles at national, state, and air basin scales, *J. Geophys. Res.*, *117*, D00V18, doi:10.1029/2012JD018304.

McDonald, B. C., D. R. Gentner, A. H. Goldstein, and R. A. Harley (2013), Long-term trends in motor vehicle emissions in U.S. Urban areas, *Environ. Sci. Technol.*, *47*, 10,022–10,031.

McDonald-Buller, E. C., et al. (2011), Establishing policy relevant background (PRB) ozone concentrations in the United States, *Environ. Sci. Technol.*, *45*, 9484–9497.

Miyazaki, K., H. J. Eskes, K. Sudo, M. Takigawa, M. van Weele, and K. F. Boersma (2012), Simultaneous assimilation of satellite NO_2, O_3, CO, and HNO_3 data for the analysis of tropospheric chemical composition and emissions, *Atmos. Chem. Phys.*, *12*, 9545–9579.

Monks, P. S., et al. (2009), Atmospheric composition change: Global and regional air quality, *Environment*, *43*, 5268–5350.

Mu, M., et al. (2011), Daily and 3-hourly variability in global fire emissions and consequences for atmospheric model predictions of carbon monoxide, *J. Geophys. Res.*, *116*, D24303, doi:10.1029/2011JD016245.

Mueller, S. F., and J. W. Mallard (2011), Contributions of natural emissions to ozone and $PM^{2.5}$ as simulated by the Community Multiscale Air Quality (CMAQ) model, *Environ. Sci. Technol.*, *45*, 4817–4823.

Nassar, R., et al. (2008), Validation of Tropospheric Emission Spectrometer (TES) nadir ozone profiles using ozonesonde measurements, *J. Geophys. Res.*, *113*, D15S17, doi:10.1029/2007JD008819.

National Research Council (NRC) (2009), *Global Sources of Local Pollution: An Assessment of Long-Range Transport of Key Air Pollutants to and From the United States*, pp. 35–66, The Natl. Acad. of Press, Washington, D. C. [Available at http://books.nap.edu/openbook.php?record_id=12743&page=35.]

Office of Air Quality Planning and Standards (2008), *Quality Assurance Handbook for Air Pollution Measurement Systems, Vol. II: Ambient Air Quality Monitoring Program*, Office of Air Quality Planning and Standards, U.S. EPA, Research Triangle Park, N.C. [Available at http://www.epa.gov/ttn/amtic/files/ambient/pm25/qa/QA-Handbook-Vol-II.pdf.]

Oltmans, S. J., A. S. Lefohn, J. M. Harris, and D. S. Shadwick (2008), Background ozone levels of air entering the west coast of the U.S. and assessment of longer-term changes, *Atmos. Environ.*, *42*, 6020–6038, doi:10.1016/j.atmosenv.2008.03.034.

Parrington, M., D. B. A. Jones, K. W. Bowman, L. W. Horowitz, A. M. Thompson, D. W. Tarasick, and J. C. Witte (2008), Estimating the summertime tropospheric ozone distribution over North America through assimilation of observations from the Tropospheric Emission Spectrometer, *J. Geophys. Res.*, *113*, D18307, doi:10.1029/2007JD009341.

Parrington, M., D. B. A. Jones, K. W. Bowman, A. M. Thompson, D. W. Tarasick, J. Merrill, S. J. Oltmans, T. Leblanc, J. C. Witte, and D. B. Millet (2009), Impact of the assimilation of ozone from the Tropospheric Emission Spectrometer on surface ozone across North America, *Geophys. Res. Lett.*, *36*, L04802, doi:10.1029/2008GL036935.

Parrish, D. D., D. B. Millet, and A. H. Goldstein (2009), Increasing ozone in marine boundary layer inflow at the west coasts of North America and Europe, *Atmos. Chem. Phys.*, *9*, 1303–1323, doi:10.5194/acp-9-1303-2009.

Parrish, D. D., K. C. Aikin, S. J. Oltmans, B. J. Johnson, M. Ives, and C. Sweeny (2010), Impact of transported background ozone inflow on summertime air quality in a California ozone exceedance area, *Atmos. Chem. Phys.*, *10*, 10,093–10,109, doi:10.5194/acp-10-10093-2010.

Parrish, D. D., H. B. Singh, L. Molina, and S. Madronich (2011), Air quality progress in North American megacities: A review, *Atmos. Environ.*, *45*(39), 7015–7025, doi:10.1016/j.atmosenv.2011.09.039.

Parrish, D. D., et al. (2012), Long-term changes in lower tropospheric baseline ozone concentrations at northern mid-latitudes, *Atmos. Chem. Phys.*, *12*, 11,485–11,504, doi:10.5194/acp-12-11485-2012.

Parrish, D. D., et al. (2014), Long-term changes in lower tropospheric baseline ozone concentrations: Comparing chemistry-climate models and observations at northern mid-latitudes, *J. Geophys. Res. Atmos.*, *119*, 5719–5736, doi:10.1002/2013JD021435.

Pechony, O., and D. T. Shindell (2010), Driving forces of global wildfires over the past millennium and the forthcoming century, *Proc. Natl. Acad. Sci. U. S. A.*, *107*, 19,167–19,170, doi:10.1073/pnas.1003669107.

Pfister, G., A. M. Thompson, L. K. Emmons, P. G. Hess, J.-F. Lamarque, and Y. E. Yorks (2008), Analysis of the summer 2004 ozone budget over the U.S. using IONS observations and MOZART-4 simulations, *J. Geophys. Res.*, *113*, D23306, doi:10.1029/2008JD010190.

Pfister, G. G., et al. (2011), Characterizing summertime chemical boundary conditions for airmasses entering the U.S. West Coast, *Atmos. Chem. Phys.*, *11*, 1769–1790, doi:10.5194/acp-11-1769-2011.
Pierce, R. B., et al. (2007), Chemical data assimilation estimates of continental U.S. ozone and nitrogen budgets during the Intercontinental Chemical Transport Experiment–North America, *J. Geophys. Res.*, *112*, D12S21, doi:10.1029/2006JD007722.
Pierce, R. B., et al. (2009), Impacts of background ozone production on Houston and Dallas, Texas, air quality during the Second Texas Air Quality Study field mission, *J. Geophys. Res.*, *114*, D00F09, doi:10.1029/2008JD011337.
Pollack, I. B., T. B. Ryerson, M. Trainer, J. A. Neuman, J. M. Roberts, and D. D. Parrish (2013), Trends in ozone, its precursors, and related secondary oxidation products in Los Angeles, California: A synthesis of measurements from 1960 to 2010, *J. Geophys. Res. Atmos.*, *118*, 5893–5911, doi:10.1002/jgrd.50472.
Pusede, S. E., and R. C. Cohen (2012), On the observed response of ozone to NO_x and VOC reactivity reductions in San Joaquin Valley California 1995-present, *Atmos. Chem. Phys.*, *12*, 8323–8339.
Richards, N. A. D., G. B. Osterman, E. V. Browell, J. W. Hair, M. Avery, and Q. Li (2008), Validation of Tropospheric Emission Spectrometer ozone profiles with aircraft observations during the Intercontinental Chemical Transport Experiment–B, *J. Geophys. Res.*, *113*, D16S29, doi:10.1029/2007JD008815.
Rodgers, C. D. (2000), *Inverse Methods for Atmospheric Sounding: Theory and Practice*, World Sci., Singapore.
Russell, A. R., L. C. Valin, E. J. Buscela, M. O. Wenig, and R. C. Cohen (2010), Space-based constraints on spatial and temporal patterns of NO_x emissions in California 2005–2008, *Environ. Sci. Technol.*, *44*, 3608–3615.
Russell, A. R., L. C. Valin, and R. C. Cohen (2012), Trends in OMI NO_2 observations over the United States: Effects of emission control technology and the economic recession, *Atmos. Chem. Phys.*, *12*, 12,197–12,209.
Sandu, A., and T. F. Chai (2011), Chemical data assimilation an overview, *Atmosphere*, *2*(3), 426–463, doi:10.3390/atmos2030426.
Schere, K., et al. (2012), Trace gas/aerosol boundary concentrations and their impacts on continental-scale AQMEII modeling domains, *Atmos. Environ.*, *53*, 38–50, doi:10.1016/j.atmosenv.2011.09.043.
Shindell, D. T., G. Faluvegi, D. M. Koch, G. A. Schmidt, N. Unger, and S. E. Bauer (2009), Improved attribution of climate forcing to emissions, *Science*, *326*, 716–718, doi:10.1126/science.1174760.
Shindell, D. T., et al. (2013), Radiative forcing in the ACCMIP historical and future climate simulations, *Atmos. Chem. Phys.*, *13*, 2939–2974, doi:10.5194/acp-13-2939-2013.
Singh, H. B., et al. (2010), Pollution influences on atmospheric composition and chemistry at high northern latitudes: Boreal and California forest fire emissions, *Atmos. Environ.*, *44*(36), 4553–4564.
Singh, H. B., C. Cai, A. Kaduwela, A. Weinheimer, and A. Wisthaler (2012), Interactions of fire emissions and urban pollution over California: Ozone formation and air quality simulations, *Atmos. Environ.*, doi:10.1016/j.atmosenv.2012.03.046.
Singh, K., M. Jardak, A. Sandu, K. Bowman, M. Lee, and D. Jones (2011a), Construction of non-diagonal background error covariance matrices for global chemical data assimilation, *Geosci. Model Dev.*, *4*, 299–316, doi:10.5194/gmd-4-299-2011.
Singh, K., A. Sandu, K. W. Bowman, M. Parrington, D. B. A. Jones, and M. Lee (2011b), Ozone data assimilation with GEOS-Chem: A comparison between 3-D-Var, 4-D-Var, and suboptimal Kalman filter approaches, *Atmos. Chem. Phys Discuss.*, *11*, 22,247–22,300, doi:10.5194/acpd-11-22247-2011.
Skamarock, W. C., J. B. Klemp, J. Dudhia, D. Gill, D. M. Barker, W. Wang, and J. G. Powers (2008), A description of the Advanced Research WRF version 3. [Available at www.mmm.ucar.edu/wrf/users/docs/arwv3.pdf.]
Smith, K. R., et al. (2009), Public health benefits of strategies to reduce greenhouse-gas emissions: Health implications of short-lived greenhouse pollutants, *Lancet*, doi:10.1016/S0140-6736(09)61716–5.
Steiner, A. L., S. Tonse, R. C. Cohen, A. H. Goldstein, and R. A. Harley (2006), Influence of future climate and emissions on regional air quality in California, *J. Geophys. Res.*, *111*, D18303, doi:10.1029/2005JD006935.
Stevenson, D. S., et al. (2006), Multimodel ensemble simulations of present-day and near-future tropospheric ozone, *J. Geophys. Res.*, *111*, D08301, doi:10.1029/2005JD006338.
Stevenson, D. S., et al. (2013), Tropospheric ozone changes, radiative forcing and attribution to emissions in the Atmospheric Chemistry and Climate Model Intercomparison Project (ACCMIP), *Atmos. Chem. Phys.*, *13*, 3063–3085, doi:10.5194/acp-13-3063-2013.
Stohl, A., et al. (2003), Stratosphere-troposphere exchange: A review, and what we have learned from STACCATO, *J. Geophys. Res.*, *108*(D12), 8516, doi:10.1029/2002JD002490.
Task Force on Hemispheric Transport of Air Pollution (TF HTAP) (2010), 2010 Final Assessment report, Part A: Ozone and particulate matter. [Available at http://www.htap.org/activities/2010_Final_Report/HTAP%202010%20Part%20A%20110407.pdf.]
The Green Book Nonattainment Areas for Criteria Pollutants (2014), Available at http://www.epa.gov/airquality/greenbook/map8hr_2008.html, accessed in October 2014.
Thompson, A. M., S. J. Oltmans, D. W. Tarasick, P. von der Gathen, H. G. Smit, and J. C. Witte (2011), Strategic ozone sounding networks: Review of design and accomplishments, *Atmos. Environ.*, *45*(13), 2145–2163, doi:10.1016/j.atmosenv.2010.05.002.
United Nations Environment Programme and World Meteorological Organization (2011), Integrated assessment of black carbon and tropospheric ozone: Summary for decision makers. [Available at http://www.unep.org/dewa/Portals/67/pdf/Black_Carbon.pdf.]
U.S. Environmental Protection Agency (2014), Policy assessment for the review of the ozone national ambient air quality standards, 2nd external review draft. [Available at http://www.epa.gov/ttn/naaqs/standards/ozone/data/20140131pa.pdf.]
van der Werf, G. R., J. T. Randerson, L. Giglio, G. J. Collatz, M. Mu, P. S. Kasibhatla, D. C. Morton, R. S. DeFries, Y. Jin, and T. T. van Leeuwen (2010), Global fire emissions and the contribution of deforestation, savanna, forest, agricultural, and peat fires (1997–2009), *Atmos. Chem. Phys.*, *10*, 11,707–11,735, doi:10.5194/acp-10-11707-2010.
van Leeuwen, T. T., and G. R. van der Werf (2011), Spatial and temporal variability in the ratio of trace gases emitted from biomass burning, *Atmos. Chem. Phys.*, *11*(8), 3611–3629, doi:10.5194/acp-11-3611-2011.
Veefkind, J. P., et al. (2012), TROPOMI on the ESA Sentinel-5 precursor: A GMES mission for global observations of the atmospheric composition for climate, air quality and ozone layer applications, *Remote Sens. Environ.*, *120*, 70–83, doi:10.1016/j.rse.2011.09.027.
Verstraeten, W. W., K. F. Boersma, J. Zörner, M. A. F. Allaart, K. W. Bowman, and J. R. Worden (2013), Validation of six years of TES tropospheric ozone retrievals with ozonesonde measurements: Implications for spatial patterns and temporal stability in the bias, *Atmos. Meas. Tech.*, *6*, 1413–1423.
Warneke, C., J. A. de Gouw, J. S. Holloway, J. Peischl, T. B. Ryerson, E. Atlas, D. Blake, M. Trainer, and D. D. Parrish (2012), Multiyear trends in volatile organic compounds in Los Angeles, California: Five decades of decreasing emissions, *J. Geophys. Res.*, *117*, D00V17, doi:10.1029/2012JD017899.
Weinheimer, A. J., J. G. Walega, B. A. Ridley, G. W. Sachse, B. E. Anderson, and J. E. Collins (1993), Stratospheric NO_y measurements on the NASA DC-8 during AASE-II, *Geophys. Res. Lett.*, *20*, 2563–2566, doi:10.1029/93GL02627.

Weinheimer, A. J., J. G. Walega, B. A. Ridley, B. L. Gary, D. R. Blake, N. J. Blake, F. S. Rowland, G. W. Sachse, B. E. Anderson, and J. E. Collins (1994), Meridional distributions of NO_x, NO_y and other species in the lower stratosphere and upper troposphere during AASE-II, *Geophys. Res. Lett.*, *21*, 2583–2586, doi:10.1029/94GL01897.

Wigder, N. L., D. A. Jaffe, F. L. Herron-Thorpe, and J. K. Vaughan (2013), Influence of daily variations in baseline ozone on urban air quality in the United States Pacific Northwest, *J. Geophys. Res. Atmos.*, *118*, 3343–3354, doi:10.1029/2012JD018738.

Wild, O., and M. J. Prather (2006), Global tropospheric ozone modeling: Quantifying errors due to grid resolution, *J. Geophys. Res.*, *111*, D11305, doi:10.1029/2005JD006605.

Yates, E. L., L. T. Iraci, M. C. Roby, R. B. Pierce, M. S. Johnson, P. J. Reddy, J. M. Tadić, M. Loewenstein, and W. Gore (2013), Airborne observations and modeling of springtime stratosphere-to-troposphere transport over California, *Atmos. Chem. Phys.*, *13*, 12,481–12,494, doi:10.5194/acp-13-12481-2013.

Yates, E. L., L. T. Iraci, D. Austerberry, R. B. Pierce, M. C. Roby, J. M. Tadić, M. Loewenstein, and W. Gore (2014), Characterizing the impacts of vertical transport and photochemical ozone production on an exceedance area, *Atmos. Environ.*, doi:10.1016/j.atmosenv.2014.09.002.

Zhang, F., et al. (2014), Sensitivity of mesoscale modeling of smoke direct radiative effect to the emission inventory: A case study in northern sub-Saharan African region, *Environ. Res. Lett.*, *9*, 075002, doi:10.1088/1748-9326/9/7/075002.

Zhang, L., et al. (2008), Transpacific transport of ozone pollution and the effect of recent Asian emission increases on air quality in North America: An integrated analysis using satellite, aircraft, ozonesonde, and surface observations, *Atmos. Chem. Phys.*, *8*, 6117–6136, doi:10.5194/acp-8-6117-2008.

Zhang, L., D. J. Jacob, X. Liu, J. A. Logan, K. Chance, A. Eldering, and B. R. Bojkov (2010), Intercomparison methods for satellite measurements of atmospheric composition: Application to tropospheric ozone from TES and OMI, *Atmos. Chem. Phys.*, *10*, 4725–4739, doi:10.5194/acp-10-4725-2010.

Zhang, L., D. J. Jacob, N. V. Downey, D. A. Wood, D. Blewitt, C. C. Carouge, A. van Donkelaar, D. B. A. Jones, L. T. Murray, and Y. Wang (2011), Improved estimate of the policy-relevant background ozone in the United States using the GEOS-Chem global model with 1/2°×2/3° horizontal resolution over North America, *Atmos. Environ.*, *45*, 6769–6776, doi:10.1016/j.atmosenv.2011.07.054.